Chapter 3

Palladium nanoparticles confined pore engineered urethane linked thiol functionalized covalent organic framework: A high-performance catalyst for Suzuki Miyuara cross-coupling reaction

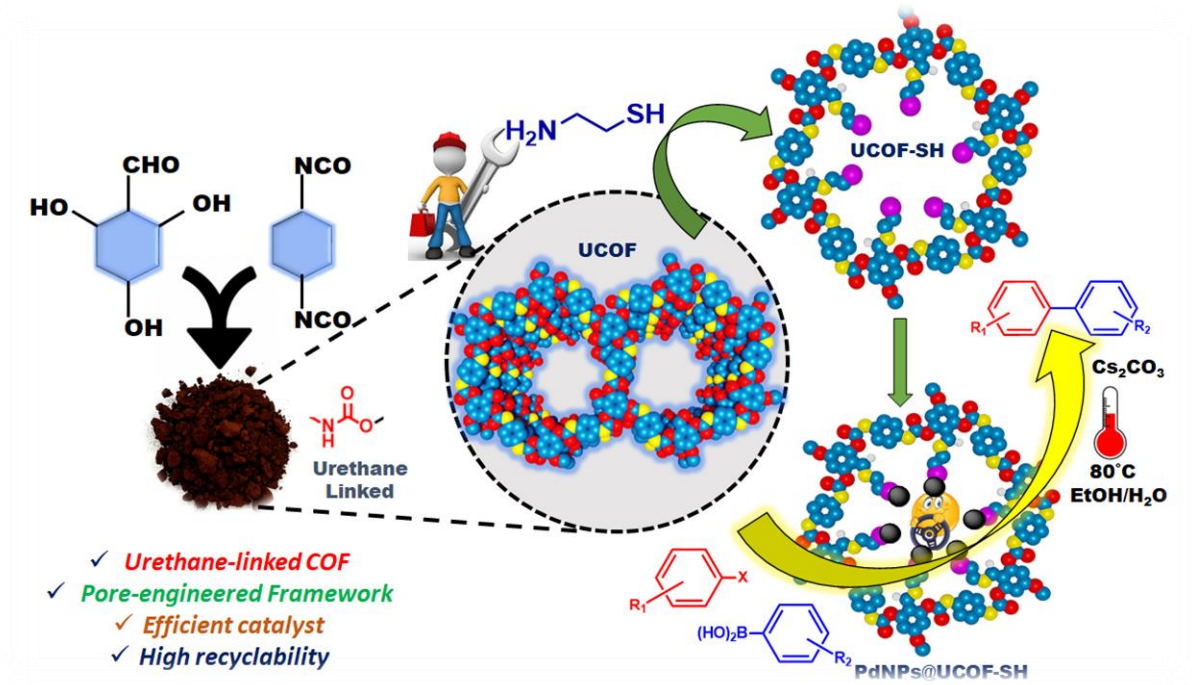

Published in *Dalton transactions*, 2023, 52, 2518-2532

3.1 Introduction

The chemical industry relies heavily on organic transformations. Among them, Suzuki Miyaura, Heck, Negishi, Stille, Kumada, Sonogashira, and other cross-coupling reactions have been widely used in synthetic organic chemistry due to their high potency for forming new carbon-carbon bonds[1]. Among various coupling reactions, the Suzuki Miyuara cross-coupling (SMC) reaction has drawn a lot of attention, due to its enormous versatility in the formation of C-C bonds. The SMC reaction is environment friendly and relatively simple to carry out. The organoborane reactants used in this reaction possess thermal stability, inertness to water and oxygen, and can tolerate diverse functional groups[2]. SMC of aryl boronic acids and aryl halides is a promising and potent method for synthesizing biaryl derivatives, which are used as building blocks in a variety of medicines, agrochemicals, polymers, and natural products[3],[4]. To date, advancement in the catalysis related to SMC reaction is of great relevance to the researchers, as it contributes to synthetic protocols for the preparation of pharmacophores as well as drug molecules[5]. In particular, various palladium (Pd) based catalysts have been exploited and gradually developed by researchers to facilitate SMC reaction.

Traditionally homogeneous palladium catalysts utilized for SMC reactions typically experience the ill effects of critical recovery issues, which leads to the wastage of valuable metal assets and additionally causes heavy metal contamination in the products. To address these issues, selective and efficient heterogeneous palladium catalysts are desired[6]. To heterogenize palladium nanoparticles, various supports have been developed by researchers such as silica, carbon materials, metal-organic framework (MOFs), metal oxide, polymers, graphene, etc. Despite its advantages, the heterogeneous catalysts experience issues such as site hiding, random and amorphous distribution, and leakage of active sites.

In recent past few years, a representative molecular platform, crystalline porous covalent organic framework (COF), has emerged as predesignable heterogeneous catalysts[7]. They have been employed as ideal options for catalytic applications, due to their remarkable characteristics such as high surface area, controllable pore size, great chemical functionalization, and excellent thermal stability [8],[9]. Since 2005, this field of covalent organic frameworks has rapidly expanded with a primary focus on two aspects, the development of new linkages/ structures and novel

applications. With the evolution of COFs, various linkages also have evolved as shown in **Figure 3.1**[10],[11]. Several reversible condensations have been employed for the synthesis of COFs such as Schiff base reaction, spiro-borane condensation, imide condensation, and Knoevenagel condensation. However, there is no report on the urethane linked covalent organic framework.

The imine bonded COFs are the most common[12]. But the reversible covalent bonds suffer a certain disadvantage, such as, under acidic conditions, the backward reaction gets accelerated, which leads to the hydrolysis of the framework. Hence, chemically nonlabile covalent bonds with more bond energies are desired to construct thermally and chemically resistant porous crystalline COFs. A urethane linkage is known to have thermal stability, hydrolytic stability, eco-safe, and high recyclability[13],[14], these properties can aid in the development of a robust and stable covalent organic framework suitable for the catalytic application.

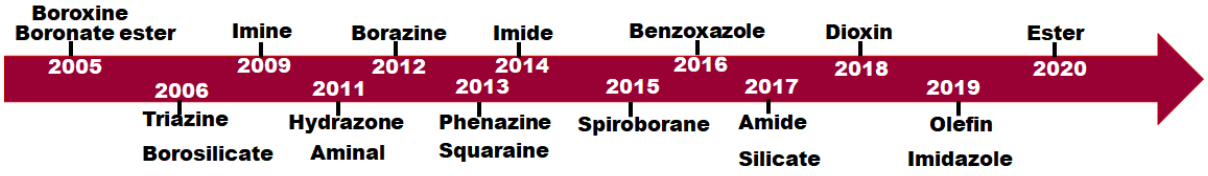

Figure 3.1: Timeline of the various covalent organic framework based on linkages

COFs exhibit many other properties that are advantageous in terms of heterogeneous catalysis. They can act as hosts for catalytically active metallic nanoparticles (NPs), minimizes the aggregation of encapsulated NPs, and large spatial separation allows multiple catalytic sites to be incorporated into the same COF[15].

In order to improve metal encapsulation performance, considerable attention has recently been dedicated to the design and synthesis of functionalized COFs. There have been two basic methodologies for designing functionalized COFs up till now. Pre-synthesis using covalent reactions of pre-designed building blocks is one technique. In recent years, a post-synthesis technique including modification of preformed COFs has received great attention[16]. COFs are designed in different ways for heterogenous catalysis **(Figure 3.2).**

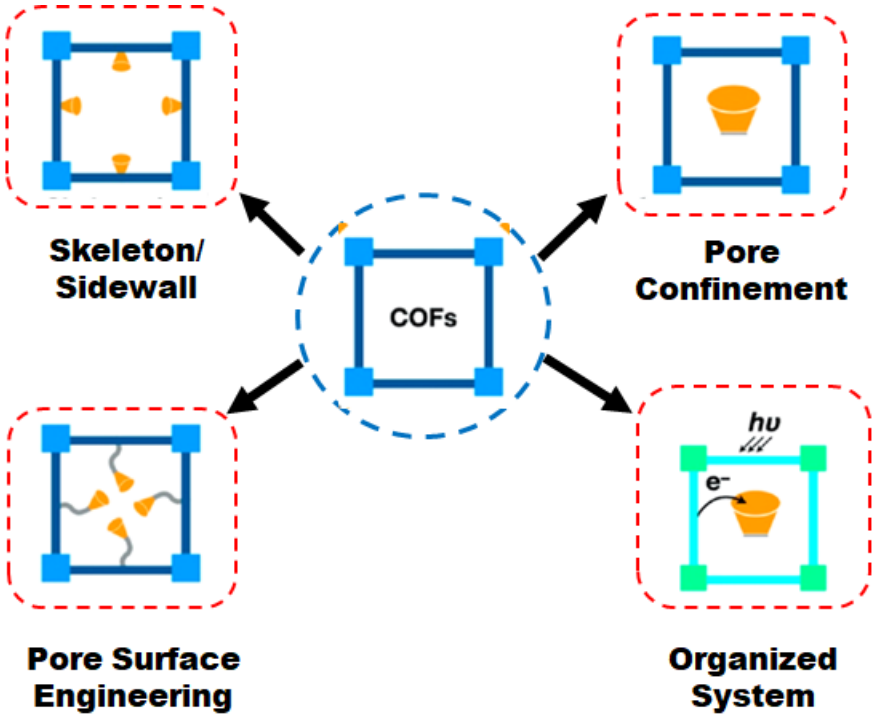

Figure 3.2: Designing of covalent organic frameworks for heterogeneous catalysis

The porosity of the COF spine becomes decreased because of this functionalization. This design principle opens up a new avenue to explore COFs as shape-selective heterogeneous catalysts to promote chemical reactions. Moreover, they have permeable channels that allow the substrate to easily access the catalytically active moieties, allowing simple and efficient chemical reactions within the catalyst. Owing to the rational pore-engineered COFs combine the features of homogenous catalysts due to enhanced selectivity, permeability and heterogenous catalysts because of their ordered structures promote mass transport while their stability and insolubility allow recycling.

This chapter envisions a rational synthesis of the urethane-based covalent organic framework using the solvothermal approach for the first time abbreviated as UCOF. The UCOF was synthesized successfully using 2,4,6-trihydroxybenzaldehyde and 1,4-phenylene diisocyanate as monomers. Because of its porous structure, the material is amenable to a wide range of systematic post-synthetic organic functionalization. Most of the COFs have been reported using triformylphloroglucinol as one of the building blocks[17], we have rationally selected monoformylphloroglucinol for the COF synthesis, which can provide a pendant formyl group for the post-modification of COF pore. The chemically programmed building blocks open up new

possibilities for the development of unique 2D or 3D multifunctional architectures. With this strategy, the cysteamine was rationally grafted onto the pendant formyl group of UCOF by a simple Schiff base condensation reaction resulting in a pore-confined UCOF-SH. Benefiting from the dangling thiol groups in the pore, functionalized UCOF can serve as the coordination sites for the transition metal cation such as Pd^{+2} due to its strong affinity towards the sulfur group. These were subsequently reduced to palladium nanoparticles. The COF minimizes the migration/coalescence of the PdNPs in the catalytic activity, guaranteeing high recyclability. Moreover, the metal nanoparticles with a pore size-driven growth have a narrow size distribution with a high surface area which ensures high catalytic activity.

The three-dimensional covalent organic frameworks and catalyst were characterized by various sophisticated analytical techniques such as CP-MAS NMR, FTIR, PXRD, BET, FESEM, HRTEM, XPS, TGA, and ICP-AES. The catalysis Suzuki Miyuara cross-coupling reaction. The catalytic efficiency was evaluated using bromobenzene and phenylboronic acid as model substrates. Starting with aryl halides and aryl boronic acids/halogenated aryl boronic acid, an excellent yield of halo-substituted and non-halo biaryl products was achieved under the optimal mild reaction conditions (80ºC, water/ethanol as solvent, and Cs_2CO_3 as an additive base). Substrate scope was investigated to understand the applicability and versatility of PdNPs@UCOF-SH. Furthermore, experiments to study leaching, regeneration, and recycling were undertaken.

3.2 Experimental Section

3.2.1 Materials

2,4,6-trihydroxybenzaldehyde (≥ 98%), and 1,4-phenylene diisocyanate (≥ 98%) were purchased from Sigma Aldrich, Mumbai, India. Cysteamine (≥ 95%), aryl boronic acid derivatives, and aryl halide derivatives were procured from TCI chemicals. Acetone, ethanol, dichloromethane (DCM), dimethyl sulfoxide (DMSO), dimethylformamide (DMF), xylene, toluene, ethyl acetate, i-propyl alcohol, methanol, Tetrahydrofuran (THF) were purchased from Sisco Research Laboratories (SRL), India. Other reagents were of analytical grade, purchased from commercial sources, and used as received without further purification. All glassware used for the studies was properly rinsed with distilled water and rinsed with acetone and then oven-dried. The visual camera picture of COF material was taken using iPhone 13 smartphone in bright daylight conditions.

3.2.2 Characterization

Nuclear magnetic resonance (^{1}H NMR). NMR studies were performed on a Bruker Avance 400 MHz spectrometer using DMSO-d6 or $CDCl_3$ as solvents and tetramethyl silane as an internal standard.

Cross Polarization/Magic Angle Spinning Nuclear Magnetic Resonance Spectroscopy. Solid-state CP-MAS NMR was recorded on NMR spectrometer (ECZR series 600 MHZ, JEOL, JAPAN) with a 3.2 mm rotor with a fast MAS (20 kHz spinning speed) probe for structural determination of the functionalized UCOF.

Fourier transform infrared spectroscopy. The chemical structure of the UCOF and its functionalized derivative was investigated by a Bruker ALPHA Fourier Transform Infrared spectrometer within a range of 4000-400 cm^{-1} with the help KBr pellets. The samples were ground with KBr and turned into pellets by disc pressing using a hydraulic pump. The spectra were recorded in the 400-4000 cm^{-1} range.

Powder X-ray diffraction (PXRD). The Powder X-ray diffraction (PXRD) patterns were recorded at room temperature on a Bruker D8 Discover X-ray diffractometer with a scattered angular range of 1-50° with an angular resolution scanning step of 0.02/sec.

Brunauer–Emmett–Teller (BET). A volumetric adsorption system (Micromeritics Instrument corporation, USA, model ASAP 2010) was used to evaluate the surface areas and porosity using N_2 adsorption/desorption isotherms at 77 K and pressures up to 1 bar. Prior to the BET measurements, the samples were activated (degassed) for 12 hours at 120°C under a vacuum. Prior to the measurements, the temperature and vacuum were maintained for 7 hours. The porosity was determined using the Barrett– Joyner–Halenda (BJH) method and the surface area was calculated using the Brunauer– Emmet–Teller (BET) method.

High-resolution transmission microscopy (HR-TEM). HRTEM was performed on FEI Technai G2, F30 microscope working at 300 kV. The palladium nanoparticles loaded with UCOF-SH solution was dispersed on carbon-coated copper grids. The sample-coated grids were then air dried overnight under ambient temperature. The imaging was then recorded on a Jeol (Jem-2100F) electron microscope at an accelerating voltage of 300 kV.

Field Emission Gun Scanning Electron Microscopy (FEG-SEM). A JSM-7600 F field emission scanning electron microscope was employed to characterize the microscopical morphologies (including surface, bottom, and, cross-section). The samples for SEM characterization were treated by spraying a thin platinum layer on their surface under vacuum conditions to enhance their

conductivity.

X-Ray Photoelectron Spectroscopy. XPS analysis was carried out on ESCA, Omicron Nanotechnology. The samples were exposed to X-rays AlKa with 1486 eV under ultra-high vacuum (UHV) conditions.

Thermogravimetric analysis: Thermogravimetric analysis (TGA) were performed using a TGA 2950 instrument in the temperature range of 25 to 750 °C under flowing N2 (30 mL min−1) with a heating rate of 10 °C min^{-1}.

Inductively coupled plasma atomic emission spectroscopy (ICP-AES). The palladium concentration in the catalyst was measured with a Simultaneous ICP Spectrometer, ARCOS, SPECTRO Analytical GmbH, Germany.

Gas Chromatography-Mass Spectroscopy (GCMS): GC-MS spectra were recorded on a Thermo Fisher Trace GC Ultra Gas Chromatograph instrument.

3.2.3 Synthesis of Urethane-based Covalent Organic Framework (UCOF)

For the synthesis of UCOF, 2,4,6-trihydroxy benzaldehyde and 1,4-Phenylene diisocyanate were used as precursors. Briefly, for the reaction, 2,4,6-trihydroxybenzaldehyde (0.77 g, 5.0 mmol) and 1,4-Phenylene diisocyanate (0.80 g, 5.0 mmol) were added in a two-necked round bottom flask containing 25ml of DMSO connected to the Dean and Stark apparatus under inert condition. Post addition, the reaction mixture was allowed to react at 120° C in an oil bath for 3 hours and then the reaction was allowed to proceed at 150° C for 72 h under continuous stirring. The coloration of the reaction mixture was changed from yellow to brown. After completion, the resulting mixture was cooled at room temperature. To this reaction mixture, 30 ml of acetone was added and sonicated for 15 min. The resulting solid was filtered using Whatmann filter paper no. 41 and washed multiple times with solvents such as acetone and DCM. The product was dried for 12 hours at 120° C in vacuo and stored in a vacuum until further use (1.238 g product was obtained).

3.2.4 Synthesis of PdNPs@UCOF-SH catalyst

The synthesis of the catalyst was carried out in two sequential steps, as follows:

Step 1: Post synthetic chemical functionalization of UCOF using Cysteamine (UCOF-SH)
UCOF pore was tailored using cysteamine via Schiff base condensation reaction resulting in imine

linkages between the pendant formyl group of UCOF and the amine group of cysteamine. Firstly, cysteamine (2 ml) was dissolved in 40 ml of methanol was added to the round bottom flask PTFE-coated magnetic stir bar. To this solution, freshly prepared UCOF (1.00 g) was added, followed by reflux at 80 º C for 16 hours under vigorous stirring. The reaction mixture was cooled to room temperature (RT). The resulting solid was filtered and washed consecutively with methanol and water. The product was dried under a vacuum at 120 º C for 6 h to obtain UCOF-SH as a dark brown powder (85%).

Step 2: Fabrication of Palladium nanoparticle confined UCOF-SH (PdNPs@UCOF-SH)

In a typical procedure, a well-dispersed suspension of as-prepared COF-SH (50 mg) in methanol (10 ml) was mixed with a solution of metal precursor i.e, $PdCl_2$ (4mg, 1.2×10^{-2} mmol) in water (2 mL). The reaction mixture was brought to dryness under a vacuum to deposit metal precursors in UCOF-SH support. This mixture was dispersed in a mixed solvent of methanol and water (10 ml, MeOH/H_2O, v/v= 3:2). A solution of $NaBH_4$ in methanol (50 mg,1.33×10^{-2} mmol) was added dropwise to the reaction mixture and stirred for 6 hours. The product was filtered, washed with ethanol followed by dichloromethane thrice, and dried under a vacuum for further use. The isolated product was dark brown in color.

3.2.5 Optimized procedure for the catalytic Suzuki Miyuara cross-coupling reaction

To assess the catalytic activity of PdNPs@UCOF-SH, the typical procedure run of SMC reaction was as follows:

A 25 mL round bottom flask containing a PTFE-coated magnetic stir bar was charged with a PdNPs@UCOF-SH catalyst (10 mg). Later, the aryl halide (0.5 mmol), the aryl boronic acid (0.75 mmol), the alkalic additive Cs_2CO_3 (325.8 mg, 1.0 mmol), and the solvent EtOH: H_2O (1:1, 5 mL) were introduced into the reaction flask. Then the reaction flask with a water condenser was transferred to the preheated oil bath stir plate at 80 °C and stirred at refluxing mode. The progress of the reaction was monitored using TLC. After the completion of the reaction, the reaction mixture was filtered to recover the catalyst. The obtained filtrate was stirred with dichloromethane (5ml) at room temperature. To this mixture, deionized water (5 ml) was added to remove the base. The obtained mixture was separated using a separating funnel and extraction was carried out thrice (3 x 5ml). The desired organic layer was obtained Vacuum evaporation was carried out to obtain the

crude product. Further, purification of the obtained crude organic product was carried out by silica gel column chromatography method using hexane/ ethyl acetate as an eluent. The isolated product was analyzed using NMR analysis.

3.2.6 Leaching and Heterogeneity test

To check the leaching, initially, the reaction was carried out in presence of a catalyst (10 mg) using a model substrate bromobenzene (0.5 mmol) and phenylboronic acid (0.75 mmol) for 1 h. Then, the reaction mixture was filtered and the obtained filtrate is allowed to react. The organic layer was extracted using dichloromethane. The extraction was done thrice (3 X 5 ml) and organic layer was dried over sodium sulfate and analyzed using GC.

3.2.7 Recycling and Regeneration of the catalyst

After the reaction was completed, the solid catalyst was recovered by the filtration separation of the mixture and the triple-wash of the solid with DCM (5 mL) and Methanol (2 ml) and dried in a vacuum oven at 100º C.

3.3 Result and Discussions

3.3.1 Synthesis and structural characterization

Herein, we report the synthesis of a urethane-linked covalent organic framework under solvothermal conditions (Monoformylphloroglucinol and 1,4-phenylene diisocyanate, DABCO as catalyst, DMSO, 120°C for 3 hours and then the temperature was raised to 150°C for 3 days), as shown in **Scheme 3.1**. The product was obtained as a brown product with an isolated yield of 90%. The obtained COF material was not soluble in water and common organic solvents such as ethanol, methanol, acetone, dichloromethane, and tetrahydrofuran.

Despite the ready and quick formation of urethane linkage, the reaction was carried out at a higher temperature for 3 days. The basic principle behind this is the breaking of existing bonds and the formation of new bonds in such a manner that leads to the self-assembly of building units eventually giving rise to frameworks. The free-formyl groups were allowed to react with cysteamine molecules to introduce dangling thiol groups in the framework skeleton.

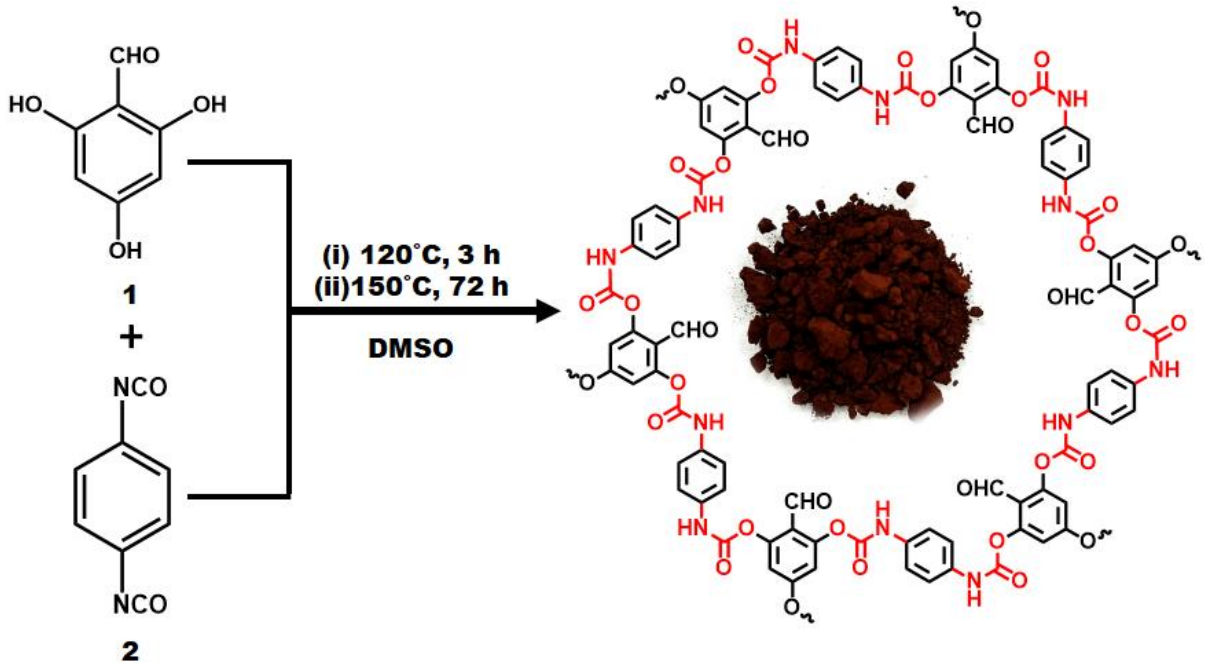

Scheme 3.1: Synthetic representation for the synthesis of a urethane-linked covalent organic framework (UCOF)

The UCOF-SH was synthesized based on a Schiff-base reaction via a solvothermal solution-suspension method. The cysteamine was introduced to improve the palladium metal encapsulation, as the cysteamine consists of the -SH group which has a great affinity to bind palladium in the porous covalent organic framework. The thiol-functionalized COF was further utilized for stabilizing the palladium nanoparticles which endowed the UCOF-SH with catalytic property due to higher surface area and small size of metal nanoparticles. Structural models for the synthetic representation of UCOF were constructed using Blender 3.2.2.0 **(Scheme 3.2).**

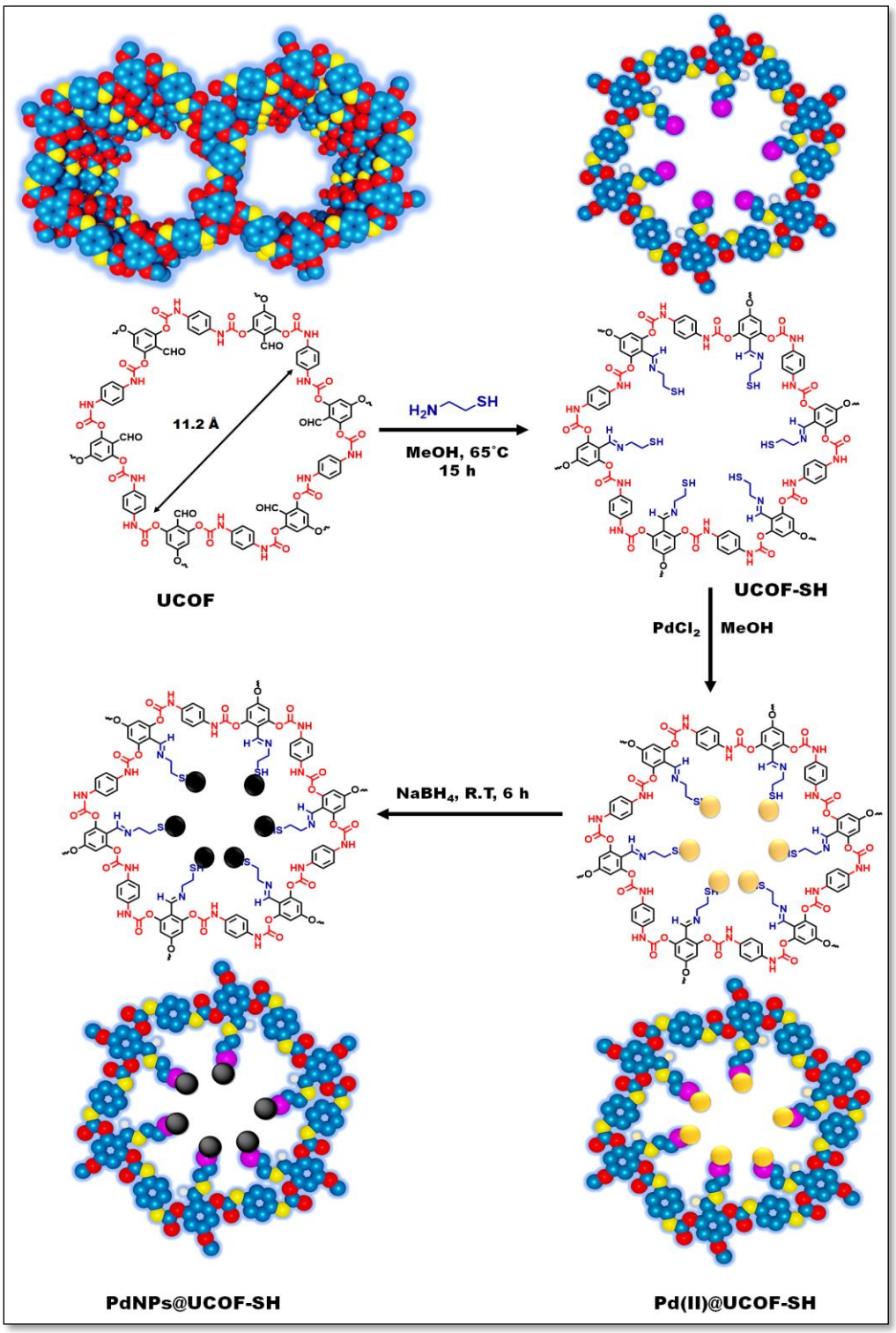

Scheme 3.2: Schematic 2D and 3D representations of the synthetic route to cysteamine functionalized pore-engineered covalent organic framework for anchoring the palladium nanoparticles

The atomic-level construction of UCOF and UCOF-SH was eventually confirmed by solid-state NMR spectroscopy. The ^{13}C cross-polarization magic-angle spinning (CP/MAS) NMR spectrum was recorded for urethane-linked parent UCOF and thiol-functionalized UCOF as shown in **Figure 3.1(A) & (B)**. The ^{13}C NMR spectra of UCOF showed a peak ~156 ppm corresponding to the carbon atom of the urethane linkage; the urethane formation is a characteristic of the condensation reaction of monoformyl phloroglucinol and phenylene diisocyanate. The signals at ~ 124.4 and 132.7 ppm can be assigned to the carbon atom of the phenyl rings, while the peak at 190 ppm indicated the presence of free-formyl groups. For UCOF-SH, the urethane carbon was observed at 156.7 ppm and the peaks at 124.7 and 133 ppm are attributed to phenyl rings[18]. Additionally, the peaks at ~38.47 ppm and 15 ppm are ascribed to the aliphatic carbon atom of the cysteamine and the disappearance of the peak corresponding to the formyl group which demonstrates the successful formation and functionalization of the UCOF network.

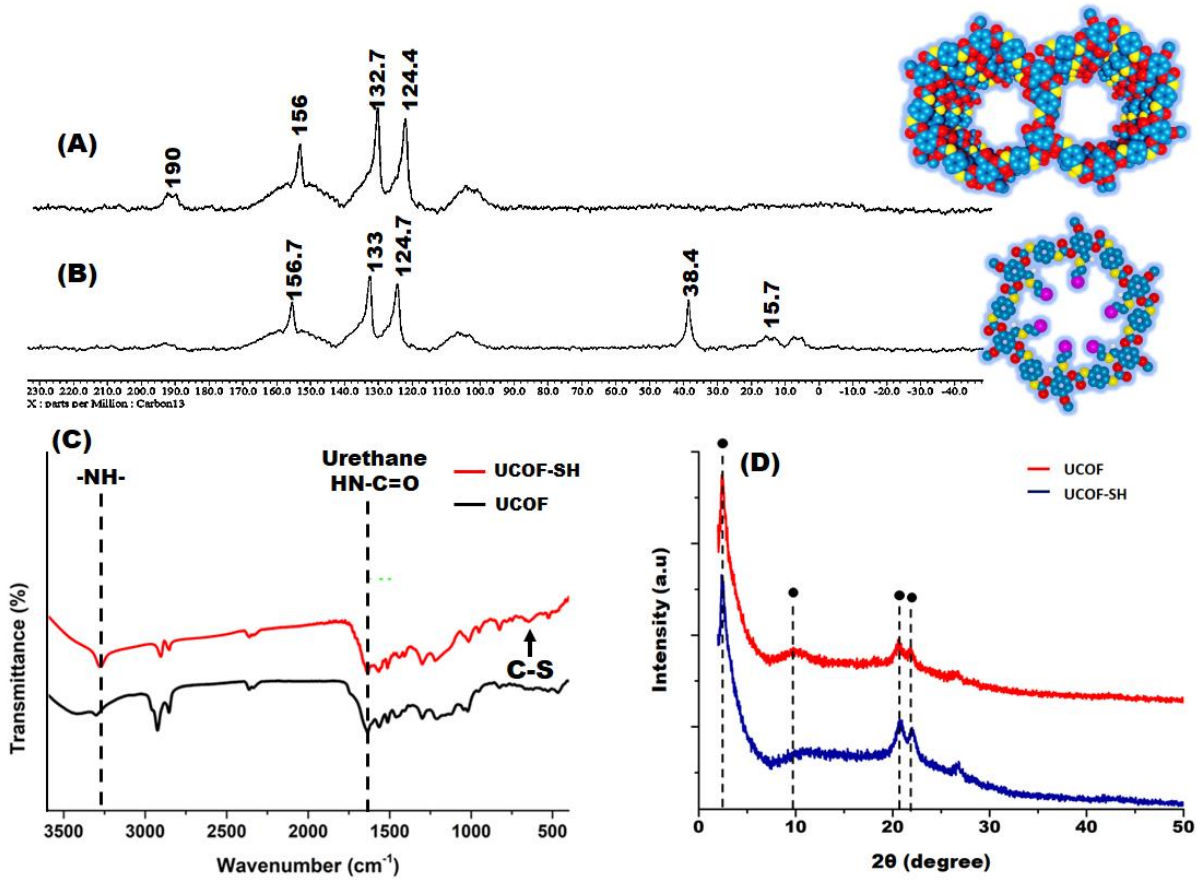

Figure 3.1: ^{13}C solid-state NMR spectra of (A) UCOF, (B) UCOF-SH (inset images showing the 3D UCOF and functionalized UCOF-SH); (C) FTIR overlay of UCOF and UCOF-SH and (D) PXRD pattern overlay of UCOF and UCOF-SH.

The successful formation of the covalent organic frameworks via urethane linkages was also confirmed using FTIR spectroscopy. As shown in **Figure 3.1(C)**, the FTIR spectra of UCOF showed the presence of characteristic -NH and carbonyl group (-CO-) of urethane at 3417.30 cm^{-1} and 1629 cm^{-1} respectively, which confirms the successful formation of urethane linkage. The merged peak in the region of 1650-1700 cm^{-1} indicated the presence of a formyl group of monoformylphloroglucinol. Additionally, the peaks observed at 1200 cm^{-1} and 1050.77 cm^{-1} correspond to the C-N and C-O stretching. The peaks observed at 1455.39 cm^{-1} ascribed to the ring stretching absorption of -C=C- of aromatic rings and the peaks at 779.77cm^{-1} and 3010.72 cm^{-1} depicted the out of plane =C-H bending and sp^2 hybridized =C-H stretching which confirms the presence of aromatic rings in the COF.

FTIR analysis validated the successful functionalization of UCOF with cysteamine. The spectra of UCOF-SH showed a presence of a secondary amine peak at 3300.87 cm^{-1} and carbonyl carbon of urethane at 1632.79 cm^{-1} which confirms the presence of urethane linkage. Due to the presence of thiol groups in COF, the C-N stretching frequency is slightly shifted to 1033 cm^{-1}. The C-S stretching frequency has a large peak at 615 cm^{-1}, indicating that COF contains thiol functionality[19].

Powder X-ray diffraction (PXRD) analysis was performed to study the crystallinity and the PXRD profile of the parent UCOF, thiol functionalized UCOF are illustrated in **Figure 3.1(D)**. The urethane-linked parent COF showed a set of intense peaks $2\theta = 3.1^{\circ}$, 10.1° which can be assigned to planes (100) and (220) respectively[20]**.** It indicates good crystallinity with a long-range ordered molecular structure and successful formation of COF[21]. The functionalized UCOF-SH and the catalyst PdNPs@UCOF-SH also showed good crystallinity with strong peaks at 3.0° and 2.8°, respectively. In UCOF-SH an intense diffraction peak at $2\theta = 27^{\circ}$ was observed, which originates from the spacing between the layer (100 planes), as previously reported for other COF-SH[22].

The EDS mapping analysis revealed the presence of the target element in the UCOF, UCOF-SH **(Figure 3.2)**, and the catalyst (**Figure 5B)**. The EDX spectrum confirmed the presence of C, O, N in the urethane-linked UCOF and C, O, N, S in the thiol-functionalized UCOF. To further validate the successful loading of palladium nanoparticles in the functionalized UCOF framework the elemental mapping of the catalyst was also carried out. The component elements Pd (3.18 wt%),

S, O, N and C are well distributed in the catalyst, which again supports the excellent dispersity of the Pd NPs in the thiol functionalized UCOF**.**

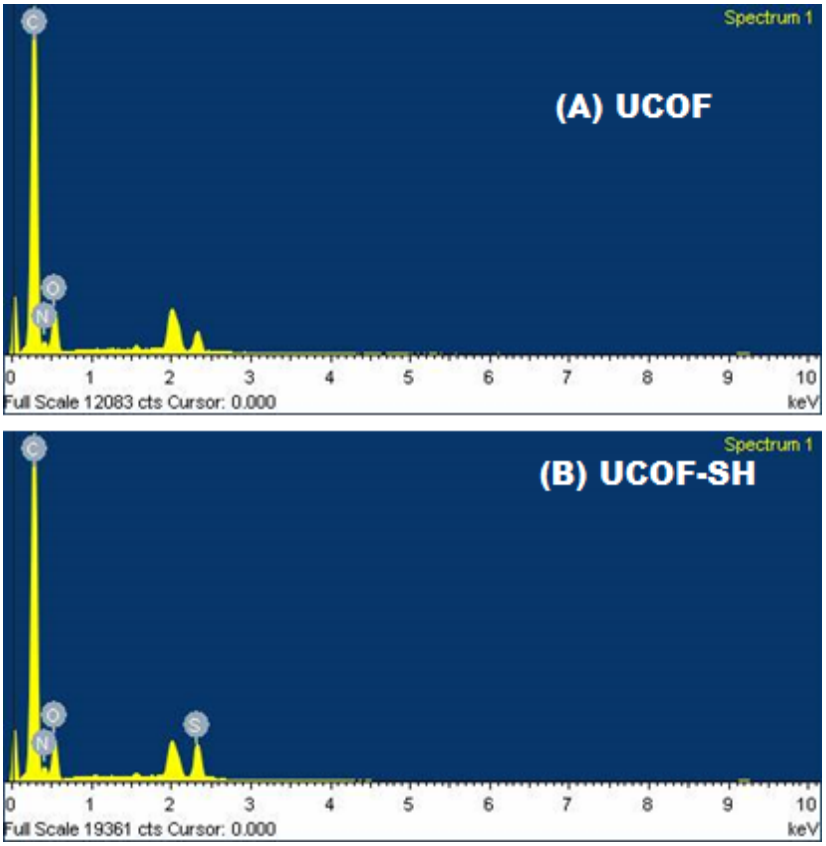

Figure 3.2: Elemental Mapping of (A) UCOF and (B) UCOF-SH

The surface area and porosity of the synthesized carriers and the catalyst were determined by nitrogen adsorption-desorption analysis **(Figure 3.3 (C), 3(D) & 4(D))**. Brunauer-Emmett-Teller surface area of UCOF, UCOF-SH, and PdNPs@UCOF-SH was calculated to be 123.6 $m^2 g^{-1}$, 69.7 $m^2 g^{-1}$, and 36.6 $m^2 g^{-1}$ and their corresponding pore volumes were 0.93 $cm^3 g^{-1}$, 0.78 $cm^3 g^{-1}$, and 0.16 $cm^3 g^{-1}$ respectively when P/P_0=0.99.

Compared to the UCOF, the surface area, pore volume, and pore size of the UCOF-SH decreased suggesting that the pores of the urethane-linked COF were occupied by the thiol groups after its post-modification with cysteamine. The relatively low surface area of UCOF-SH is probably due to the thin layers or small domains of the COF material, similar to the case reported by Zhang on the high crystalline COF with low porosity[23],[21]. The pore width was calculated using Barret-

Joyner-Halenda analysis, 26.8 nm (UCOF), 12.6 nm (UCOF-SH), and 9.2 nm (PdNPs@UCOF-SH), which belongs to a mesoporous region[24]**.** The adsorption curve showed a type IV adsorption isotherm, indicating that it is a mesoporous material[20]. Pore size distribution calculated from BJH method showed the synthesized COF materials belong to mesoporous region. The results of the BET analysis were supported by the FESEM images shown in **Figure 3.3**.

The morphology of COF showed a porous structure containing uniform and nanometer-sized fibers. Post-modification with cysteamine, a decrease in pore size and slight change in morphology along with porous surface was observed in the SEM micrographs.

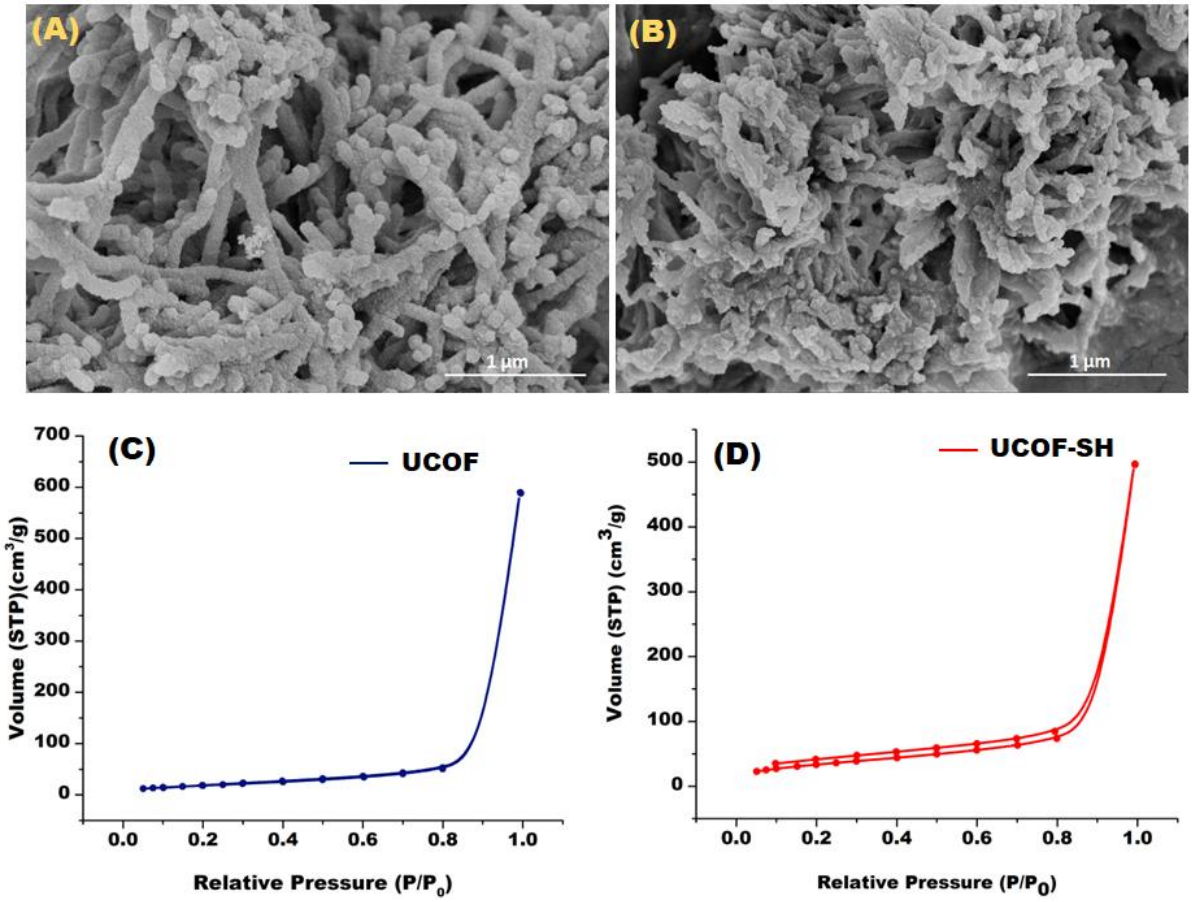

Figure 3.3: SEM images of (A) UCOF, (B) UCOF-SH; Nitrogen adsorption-desorption isotherm of (C) UCOF and (D) UCOF-SH.

In addition, we examined the size and dispersion of Pd NPs in thiol-functionalized COF using high-resolution transmission electron microscopy (HRTEM). The typical TEM images of the PdNPs@UCOF-SH **(Figure 3.4 (A)**) revealed that the small Pd NPs were uniformly distributed in the carrier. The size distribution of Pd NPs in catalyst was calculated by measuring more than 50

randomly chosen particles from the TEM images. The small Pd NPs has an average size of 4-6 nm particle size with a narrow size distribution **(inset in Figure 3.4 (A)).** It was also confirmed that the Pd NPs are in the crystalline phase with a crystal plane spacing of 0.24 nm, which corresponds to the (111) plane of the Pd NPs **as shown in Figure 3.4 (B).**

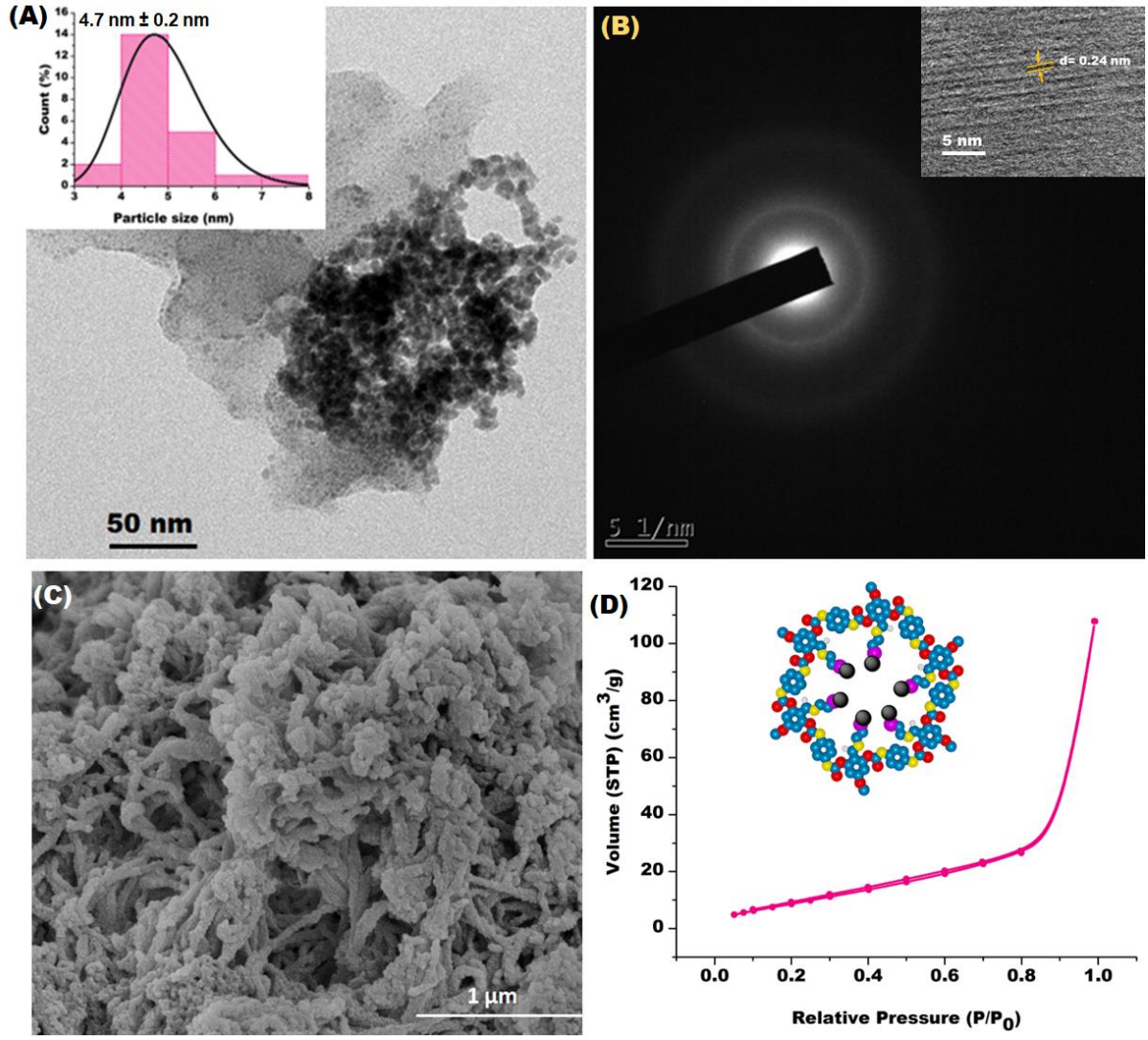

Figure 3.4: Characterization of PdNPs@UCOF-SH catalyst (A) high-resolution TEM image, the inset is the size distribution profile of Pd NPs; (B) selected area electron diffraction (SAED) pattern; the inset is the interlayer d spacing (C) SEM image and (D) Nitrogen adsorption-desorption isotherm.

To further illustrate the oxidation state of the loaded palladium nanoparticles species after reduction and corresponding chemical bonding states in PdNPs@UCOF-SH were investigated

using XPS analysis. In the full range XPS spectrum of the PdNPs@UCOF-SH catalyst: C 1s, O 1s, N 1s, S 2p, and Pd 3d components were observed, as shown in **Figure 3.5.** The binding energy range in the high-resolution C 1s XPS spectra was about 284–288 eV. The high-resolution C 1s spectrum as observed from the XPS analysis was resolved into four characteristic peaks. Briggs and Seah stated that the binding energy value of C 1s for any form of hybridization, C-C/C-H, is equal to 285.0 eV; at the same time, oxygen causes a shift in the binding energy values, and the C 1s becomes equal to 285.4 for C=O bonding[25]**.**

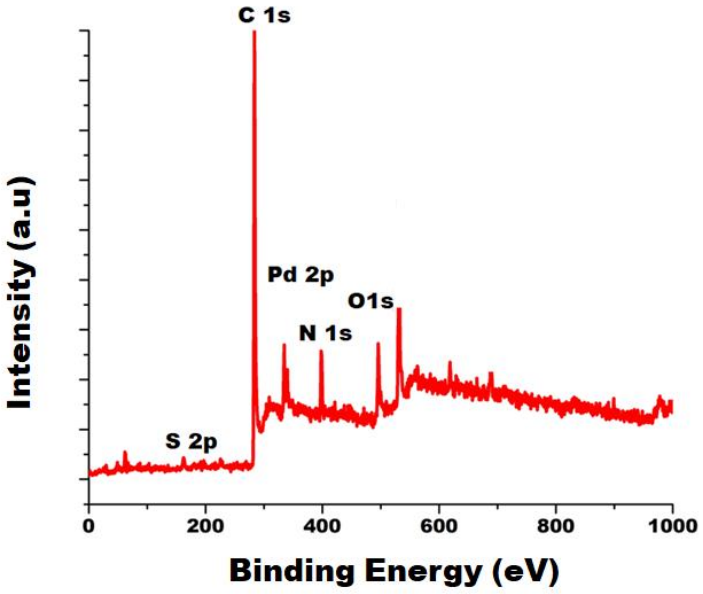

Figure 3.5: Full scan XPS spectrum of PdNPs@UCOF-SH catalyst

The observed deconvoluted peaks at 284.5, 284.6, 285.4, and 286.5 were attributed to the functional groups of C-C/C-H, C=O, C-N, and C-O, respectively, in the COF framework[15]. The N 1s spectra can be deconvoluted into a single sharp peak in the range of 399.9−400.1 eV for PdNPs@UCOF-SH, which corresponds well with the imine and urethane linkage in the catalyst[26]. The O 2p deconvoluted spectra showed two peaks at 531.5 ± 0.2 eV and 535.4± 0.2 eV attributed to the C=O and C-O-C linkages, respectively[15]. **Figure 3.6 (D)** demonstrated two peaks for S 2p1/2 at 163.1 eV and 165.9 eV. The peak at 165.9 eV was attributed to a characteristic peak of C-S indicating successful functionalization of the framework with cysteamine units[27]. Moreover, this peak demonstrates the unbound thiol group. The peak at 163.1 eV was observed due to the strong interaction of Pd-S suggesting the successful loading of Pd nanoparticle loading

in the functionalized COF matrix.

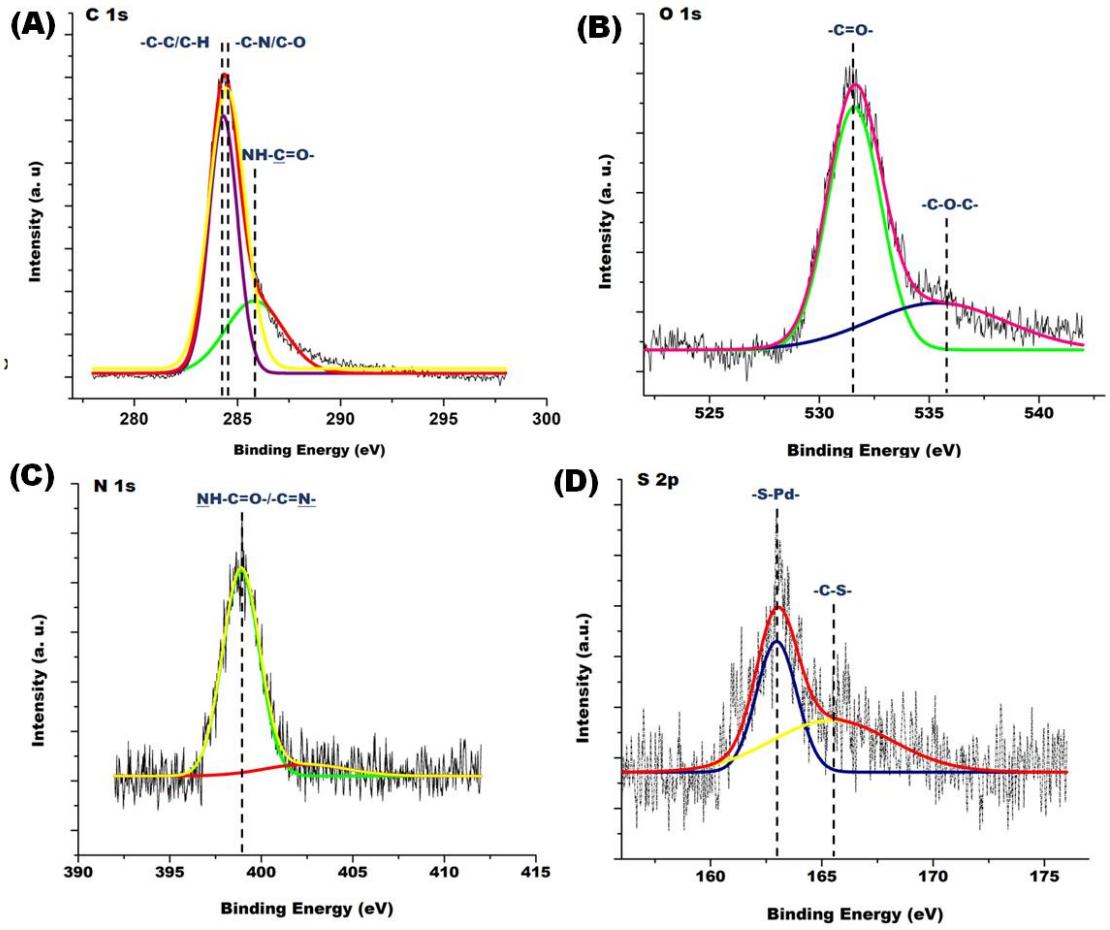

Figure 3.6: Deconvulated XPS spectra of (A) C 1s (B) O 1s (C) N 1s and (D) S2p

Moreover, the deconvoluted XPS spectrum of the PdNPs showed two strong peaks at 335.1 and 340.6 eV, which were assigned to Pd 3d5/2 and 3d3/2 binding energies, respectively **(Figure 3.7)**[28]**.** The result demonstrated that all the Pd elements anchored in the COF framework were present in a zerovalent oxidation state [29]**.**

In the case of PdNPs@UCOF-SH showed a peak at 40.43 due to (111) planes having high intensity as shown in **Figure 3.7(C).** This confirms that Pd metal is in a zero-oxidation state. The emergence of a new peak in the XRD pattern on loading Pd indicates the presence of dispersed Pd nanoparticles in the COF which can act as catalytic sites for the organic transformation. The basic XRD pattern of the COF did not exhibit any significant change after functionalization (UCOF-SH) and also after loading of palladium nanoparticles (PdNPs@UCOF-SH) as can be seen in **Figure 3.7(D) & 3.7(C).** This phenomenon suggests that functionalization and palladium metal loading

preserve overall crystallinity and structural stability of the host framework**.**

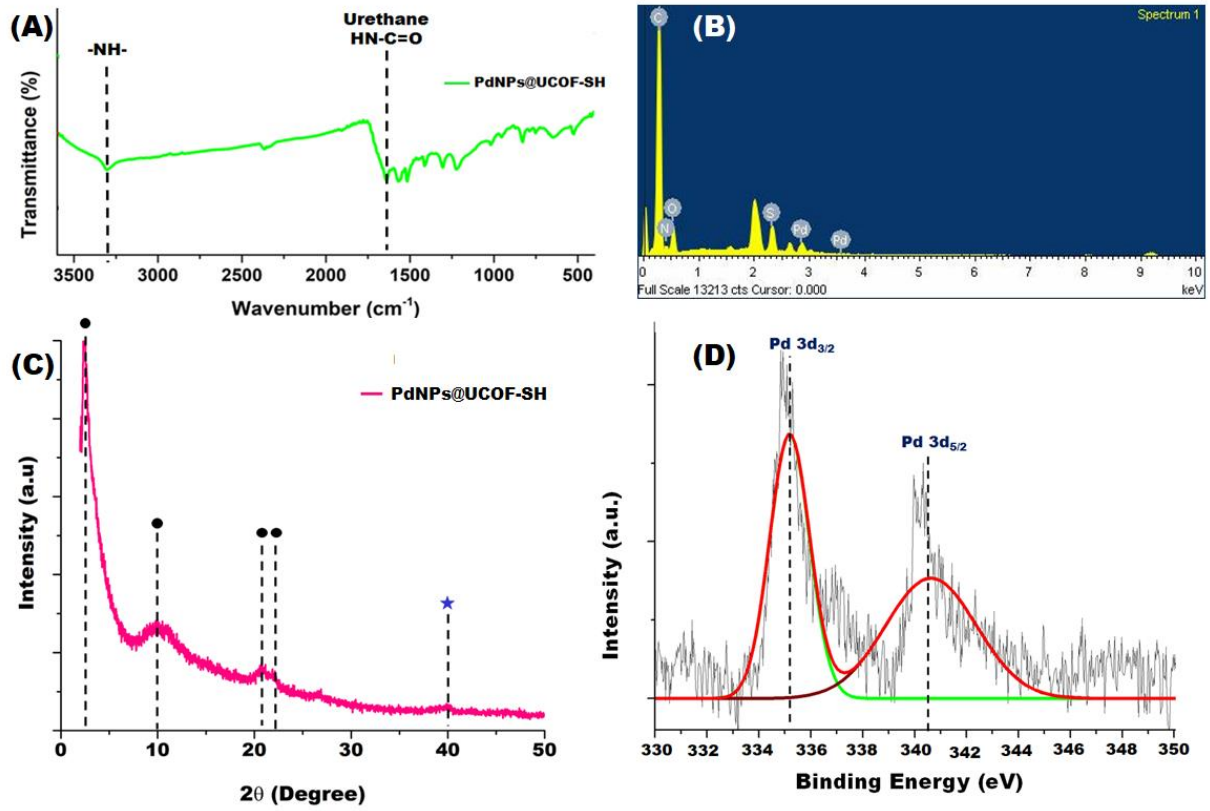

Figure 3.7: Characterization of PdNPs@UCOF-SH (A) FTIR spectrum (B) Elemental Mapping (C)PXRD profile and (D) XPS spectrum of deconvoluted Pd 3d.

The thermogravimetric analysis of the UCOF and the catalyst indicates high thermal stability upto 300-350 ºC (**Figure 3.8 (A) & 3.8 (B)**). The inductively coupled plasma (ICP) analysis revealed the palladium content in the catalyst was 4.08 %.

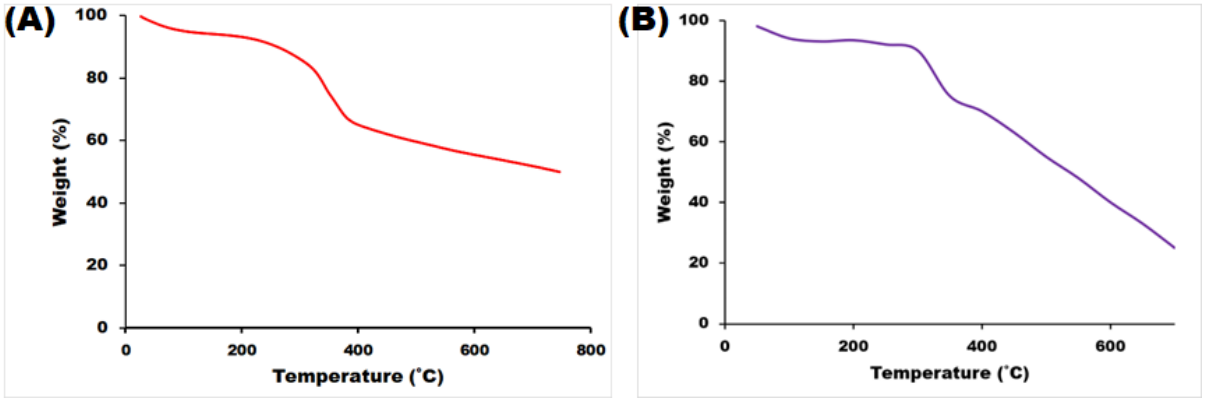

Figure 3.8: TGA plot of (A) UCOF and (B) PdNPs@UCOF-SH

3.3.2 Catalytic application of PdNPs@UCOF-SH

Captivating the advantage of pore-engineered UCOF and highly confined small palladium nanoparticles, PdNPs@UCOF-SH were employed as a catalyst for the Suzuki-Miyaura cross-coupling reaction.

The investigations began with the initial optimization to assess the activity of our heterogenous catalyst towards the Suzuki-Miyaura cross-coupling reaction using bromobenzene and phenylboronic acid as model substrates. In the recent past, various palladium-loaded covalent organic framework-based catalysts have been reported for the Suzuki coupling reaction. However, its potential application in industry is still limited due to leaching of palladium ion into the reaction mixture from the large pores of the COF and the low reactivity of the catalyst due to stronger interaction with the COF backbone limits its reusability and recyclability**.** Employment of pore-confined COFs can help to overcome palladium leaching by providing stability, reactivity, and increased accessibility to the reactants.

In the benchmark reaction of bromobenzene and phenylboronic acid, the dosage of catalyst, solvents, and base was optimized. However, the employment of harmful organic solvents and ligands, expensive homogenous catalysts, severe reaction conditions, catalyst stability, low product yield, and recyclability are significant limitations in the majority of the reported work.

The prepared heterogeneous catalyst was employed to make a comparison of this reaction in xylene solvent under previously reported standard reaction conditions[30]**,** the results are summarized in **Table 3.1.** Like other previously reported COF-supported palladium catalysts, our prepared catalyst also demonstrated moderate reactivity and good yield under similar reaction conditions which can be due to the small size of PdNPs supported by pore-engineered UCOF[31].

Here, our emphasis was placed on the use of green solvents to substitute the organic solvents and milder reaction conditions. The results are summarized in **Table 3.1.**

Table 3.1: Optimization of reaction conditions for Suzuki Miyuara Cross-Coupling reaction

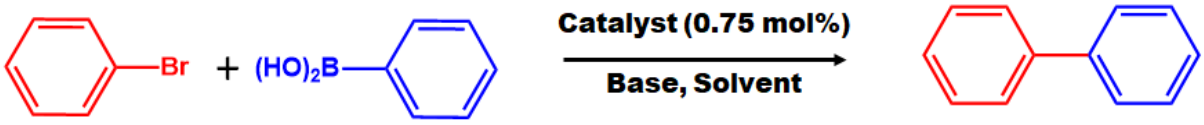

Entry	Catalyst	Additive	Solvent	Temperature	Time	%Yield [a] (±2)
1	UCOF	K_2CO_3	Xylene	150	24	-
2	PdNPs@UCOF	K_2CO_3	Xylene	150	3	80
3	PdNPs@UCOF-SH	K_2CO_3	Xylene	150	3	95
4	PdNPs@UCOF-SH	K_2CO_3	DMF	150	3	10
5	PdNPs@UCOF-SH	K_2CO_3	THF	70	3	15
6	PdNPs@UCOF-SH	K_2CO_3	MeOH	100	3	80
7	PdNPs@UCOF-SH	K_2CO_3	EtOH	80	3	85
8	PdNPs@UCOF-SH	K_2CO_3	Toulene	120	3	70
9	PdNPs@UCOF-SH	K_2CO_3	Water	100	3	30
10	PdNPs@UCOF-SH	K_2CO_3	i-PrOH	90	3	57
11	PdNPs@UCOF-SH	K_2CO_3	DCM	50	3	42
12	PdNPs@UCOF-SH	K_2CO_3	Acetone	60	3	30
13	PdNPs@UCOF-SH	K_2CO_3	EtOH/H_2O	100	3	90
14	PdNPs@UCOF-SH	K_2CO_3	EtOH/H_2O	80	3	96
15	PdNPs@UCOF-SH	Na_2CO_3	EtOH/H_2O	80	3	90
16	PdNPs@UCOF-SH	$N(Et)_3$	EtOH/H_2O	80	3	42
17	PdNPs@UCOF-SH	NaOH	EtOH/H_2O	80	3	30
18	PdNPs@UCOF-SH	KOH	EtOH/H_2O	80	3	50
19[b]	PdNPs@UCOF-SH	Cs_2CO_3	EtOH/H_2O	80	3	98
20[c]	**PdNPs@UCOF-SH**	**Cs_2CO_3**	**EtOH/H_2O**	**80**	**2**	**99(100)**
22	PdNPs@UCOF-SH	Cs_2CO_3	EtOH/H_2O	35	2	88
23	PdNPs@UCOF-SH	Cs_2CO_3	EtOH/H_2O	100	2	99

Reaction Conditions: Bromobenzene (0.5 mmol), phenylboronic acid (0.75 mmol), 1.0 mmol of additive, 0.75 mol % of PdNPs@UCOF-SH (10 mg), and 5 mL of solvent. [a]Isolated Yield, [b, c] Determined by ^{1}H NMR spectroscopy based on aryl halide and GCMS (selectivity is shown in parenthesis).

To establish the importance of catalysts for the target reaction, various control experiments were performed. The model reaction was performed using native UCOF as well as UCOF-SH without palladium nanoparticles loading. As it can be concluded from the results, the coupling reaction does not proceed without palladium catalysis **(Table 3.1, entry 1).**

Furthermore, two control catalysts with similar PdNPs loadings including native COF-supported PdNPs catalyst i.e, PdNPs@UCOF and cysteamine functionalized COF-supported PdNPs catalyst i.e, PdNPs@UCOF-SH were prepared. Both the catalysts were utilized for the model reaction, however, in similar conditions, the yields of the product in the case of PdNPs@UCOF and PdNPs@UCOF-SH were 80% and 95%, respectively, **(Table 3.1, entries 2-3).**

To investigate the effect of catalyst dosage on the reaction time, the reaction was carried out with varying amounts of catalyst. The most promising catalytic activity was achieved when the 10 mg dosage of the catalyst (**Figure 3.9**).

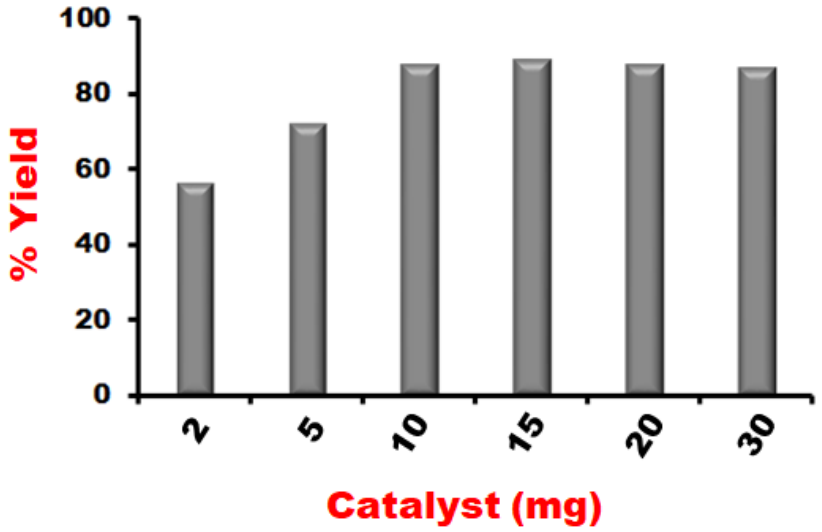

Figure 3.9: Effect of catalyst loading (Reaction Condition: Bromobenzene (0.5 mmol), phenylboronic acid (0.75 mmol), 1.0 mmol of Cs_2CO_3, (x mg) PdNPs@UCOF-SH, and solvent EtOH: H_2O 5 mL, Isolated Yield).

The base plays a critical role in Suzuki Miyuara cross-coupling reaction because it converts the boronic acid into its respective organoborate, which boosts boronic acid's reactivity towards the Pd-halide complex. Hence, the rate of transmetallation between organoborane reagents and metal halides is accelerated by the addition of base additive. The effect of base additive on the reaction was studied as depicted in **Table 3.1, entries (14-19).** From the obtained results it can be concluded that different bases showed different reactivity towards. It has been observed that the yield of the product is higher when the reaction was carried out in presence of inorganic bases compared to organic base such as triethylamine **(Table 3.1, entry 16)**. However, the yield decreased and sticky products were obtained when the reaction was carried out in presence of strong base additives such as KOH and NaOH (**Table 3.1, entries 17&18).** Furthermore, when the reaction was carried out in presence of K_2CO_3 and Cs_2CO_3, the yield was found to be 96% and 98% respectively (**Table 3.1, entries 14&19)**. The product yield was slightly decreased when the reaction was carried out using Na_2CO_3 as a base **(Table 3.1, entry 15).** Under base evaluation, Cs_2CO_3 showed the best catalytic performance. It was observed that the cesium carbonate worked quite well under this reaction conditions due its specific characteristics of the cesium cation such as its large ionic radius, low charge density, and high polarizability[2].

The reaction was carried out using model substrates in a series of solvents such as xylene, dimethylformamide, tetrahydrofuran, methanol, ethanol, water, isopropyl alcohol, dichloromethane, acetone as shown in **Table 3.1.** It was observed that when neat ethanol was used as a solvent the highest yield of the product was obtained compared to other solvents. These results are well in agreement with the reported results in the literature[32], which demonstrates that polar solvents give the best results for coupling reactions. Hence, we proceed with ethanol as a best-suited solvent for further study.

Further, we were interested to explore the influence of the EtOH: H_2O ratio on the cross-coupling reaction, and the data is shown in **Figure 3.10.** It was observed that there was a rise in the % yield of the product when the solvent system was switched from neat ethanol to EtOH: H_2O in various ratios. The greater solubility of the base in water led to this trend observation. However, due to the poor solubility of the organic substrates in water, the % yield of the product was the least when the reaction was carried out in neat H_2O.

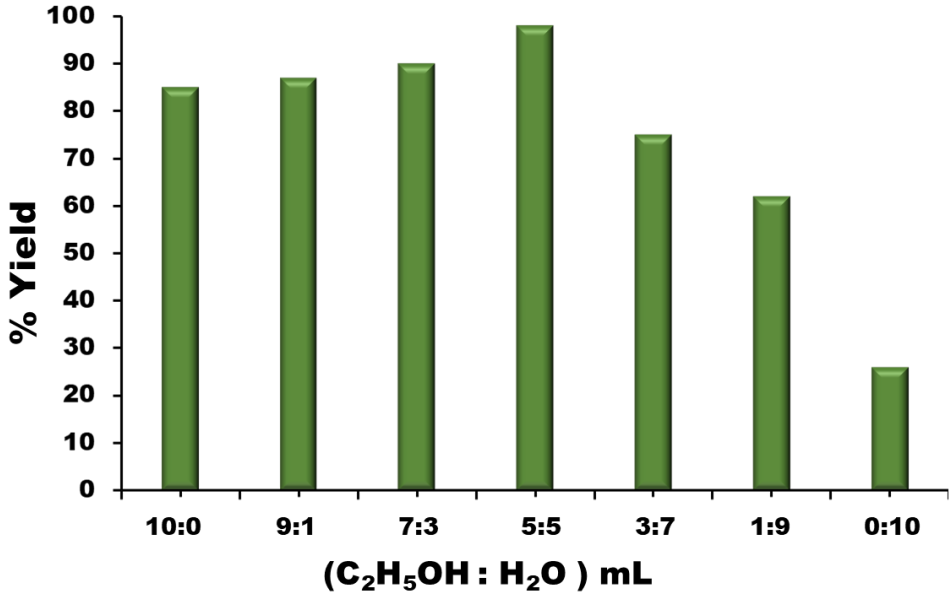

Figure 3.10: Effect of EtOH: H_2O (v/v) ratio as a solvent on cross-coupling reaction (Reaction Conditions: Bromobenzene (0.5 mmol), phenylboronic acid (0.75 mmol), 1.0 mmol of Cs_2CO_3, 0.75 mol % of PdNPs@UCOF-SH, and solvent EtOH: H_2O 5 mL, Isolated Yield).

Herein, the water, which serves as a co-solvent, might speed up the reaction and results in a high product yield. This is anticipated because the presence of water makes the ionization process of cesium carbonate easy which aids the reaction with a basic medium. The reaction was also carried out at different temperatures (**Table 3.1, entries 21, 22, and 23**), it can be seen with the increase in temperature the product yield also increases, but the maximum yield was achieved at 80°C. Further, an increase in temperature does not show any change in the product yield. Satisfactorily, the catalyst achieved excellent yield (99%) and selectivity (100%) by using cesium carbonate as the base at 80 °C for 4.0 h in water/ethanol (1:1) mixed solvent. The coupled product was monitored using TLC and analyzed using GCMS as well as NMR (**Table 3.1, entries 19-21).**

The comparative studies among various catalysts utilized for Suzuki-Miyuara cross-coupling reactions and the present work are summarized in **Table 3.2.**

Table 3.2: Comparison of Catalytic Activity and Recyclability of PdNPs@UCOF-SH with Other heterogeneous Catalysts in the Suzuki−Miyaura Reaction

Sr. No	Pd Catalyst Supports	Catalyst conc.	Solvent/ base/ temp (˚C)	Time (h)	% conversion	Recycle	Ref
1	Pomegranate Bionanocellulose	10 wt%	H_2O: EtOH/K_2CO_3/ 70	4	95	4	[32]
2	COF-LZU1	0.5 mol%	p-xylene/ K_2CO_3/150	1	96	4	[30]
3	Ionic porous organic framework	1 mol%	H_2O: EtOH/ K_3PO_4/85	2	94	5	[33]
4	COF-NHC	0.5 mol%	H_2O /K_2CO_3/r.t	1	99	8	[34]
5	Imine linked COF	10 wt%	THF/ K_2CO_3/80	2	51	-	[35]
6	MOF	2 mol%	Toulene/ K_2CO_3/90	12	96	4	[36]
7	Porous copolymer	2.5 mol %	EGME: water/ K_2CO_3/	24	92	5	[37]
8	Thioether containing COF	0.1 mol %	DMF: H_2O/ K_2CO_3/50	3	85.7	5	[21]
9	COF-SMC2	0.5 mol %	EtOH/ Cs_2CO_3/ 80	1	96	3	[31]
10	**PdNPs@UCOF-SH**	**0.75 mol%**	**EtOH: H_2O / Cs_2CO_3/ 80**	**2**	**99**	**10**	**This Work**

Under the optimal reaction conditions, the reactivity of different aryl halides (X=I, Br, Cl) with phenylboronic acid and its derivatives were studied. In this present work, the focus was directed toward the reactivity of various aryl bromides coupling with phenylboronic acid and its derivatives. The results are summarized in **Table 3.3.** The isolated products were characterized by ^{1}H NMR spectroscopy **(Figure S 1- S 10).**

Table 3.3: Scope of Suzuki cross-coupling reaction catalyzed by PdNPs@UCOF-SH

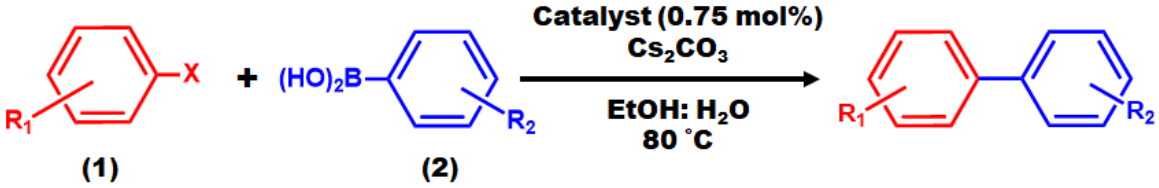

(1) (2)

Sr. No.	Aryl halide (1)	Aryl halide	Aryl boronic acid (2)	Time (h)	%Yield
1	R1=H	X=I	R2=H	**1**	**99**
2	R1=H	X=I	R2=OCH_3	**0.5**	**98**
3	R1=H	X=Br	R2=H	**2**	**99**
4	R1=OCH_3	X=Br	R2=H	**3**	**97**
5	R1=OCH_3	X=Br	R2=OCH_3	**2**	**97**
6	R1=$COCH_3$	X=Br	R2=H	**5**	**89**
7	R1=PhCN	X=Br	R2=F	**6**	**50**
8	R1=(NO_2)	X=Br, F	R2=F	**8**	**68**
9	R1=CH_3	X=Cl	R2=H	**7**	**80**
10	R1=CH_3	X=Cl	R2=F	**10**	**72**

Reaction Conditions: Aryl halide (0.5 mmol), arylboronic acid (0.75 mmol), 1.0 mmol of Cs_2CO_3, 0.75 mol % of PdNPs@UCOF-SH, and solvent EtOH: H_2O (1:1) 5 mL. [a]Isolated Yield.

The majority of substrates were converted to the target biaryl products very efficiently with the help of the PdNPs@UCOF-SH catalyst. It can be indicated from the results that iodobenzene reacted faster with phenylboronic acid (1h, 99%) than bromobenzene (1h, 99%). In the case of 4-methylchlorobenzene (7 h, 80 %), the product yield was lesser, which was improved by increasing the reaction time. The low reactivity of aryl chloride was observed compared to aryl iodide and aryl bromide as the bond energy of C-Cl is higher than C-Br/ C-I (C-Cl> C-Br> C-I). It is noteworthy that despite of lower reactivity of aryl chlorides than the aryl iodide and bromide, the biaryl product was obtained in good yield **(Table 3.3, entry10).** We also carried out the reaction using 4-fluorophenylboronic acid and aryl bromide /aryl chloride derivative, it was observed the reaction was completed in 8h/10h with 68 %/ 72% yield. From these observations, it can be predicted that the aryl halide with an electron-donating group was found to be more reactive than the counterpart having an electron-withdrawing group (**Table 3.3).**

Furthermore, we also attempted the reaction with the large-sized biphenyl bromide and phenylboronic acid under optimal reaction conditions, we obtained a low yield compared to other aryl bromides. Compared with bromobenzene and 4-bromoanisole, the reaction rate of the 4-bromo-4'-cyanobiphenyl decreased to 50% yield in the same reaction conditions, respectively **(Table 3.3, entry 8).** This can be attributed to the fact that the reactant's size and space position also impact the kinetics of the reactions [31].

From these observations, it can be predicted that the reason for the highly efficient catalytic activity as well as the versatility of PdNPs@UCOF-SH catalyst can be attributed to the presence of a large number of active sites in the pore-engineered covalent organic framework, as well as the small size and high surface area of the palladium nanoparticles. The rational post-modification of UCOF with cysteamine enhances the stability of the palladium catalyst and makes the Pd NPs disperse evenly preventing agglomeration[38]**.**

3.3.3 Recycling and regeneration studies

The homogenous palladium-based catalyst has some drawbacks that restrict its potential for industrial use, including toxicity, challenging separation, difficult recyclability, and reusability. In this situation, Pd-based heterogeneous catalysts are favored primarily for industrial production because they can be easily recycled and recovered, which lowers operating costs and prevents undesirable traces of harmful metals from appearing in the finished goods.

As our synthesized catalyst is heterogeneous in nature, the recyclability of PdNPs@UCOF-SH was also examined (**Figure 3.11).** After each catalytic run, the solid catalyst was readily recovered by filtration, washed with ethanol and dichloromethane, and then dried at 100 °C in a vacuum oven for the next catalytic run under the same reaction conditions using bromobenzene and phenylboronic acid. The yield was still up to 99%, even after the 8^{th} cycle. The yield slowly decreases after the 8^{th} cycle due to the agglomeration of palladium nanoparticles. The stability of the catalyst was measured by successive batch experiment. As shown in **Figure 3.12,** the conversion of bromobenzene did not change upto 8 cycles. To investigate the changes in the structure and morphology of the catalyst after 10 successive runs, the recycled catalyst was characterized by HRTEM, FEG-SEM, PXRD, FTIR, and EDS analysis as shown in **Figure 3.13.**

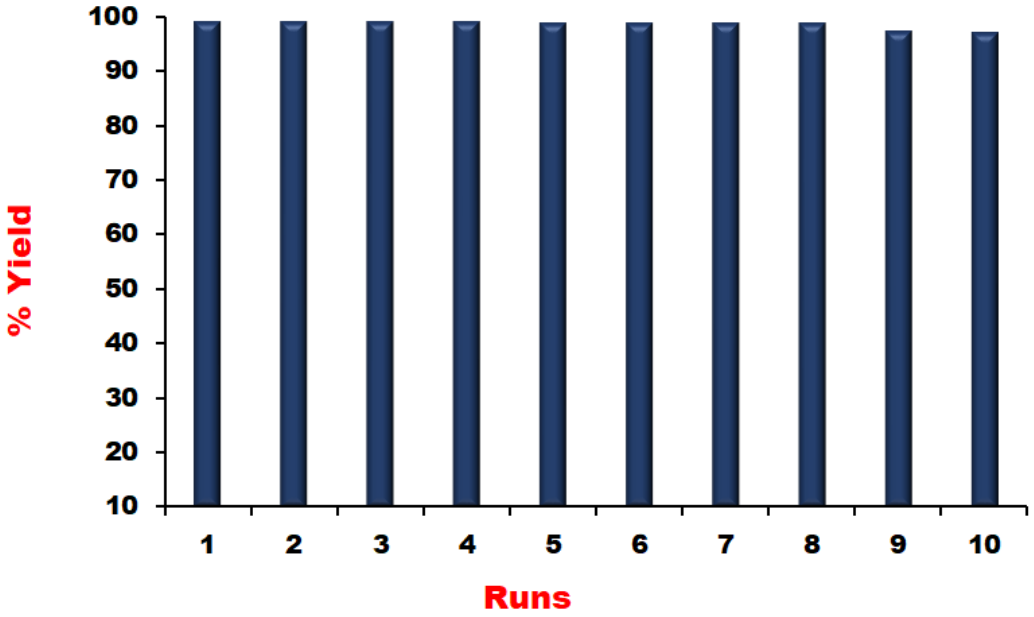

Figure 3.11: Recycling study (Reaction Conditions: Bromobenzene (0.5 mmol), phenylboronic acid (0.75 mmol), 1.0 mmol of Cs_2CO_3, 0.75 mol % of PdNPs@UCOF-SH, and solvent EtOH: H_2O 5 mL, Isolated Yield).

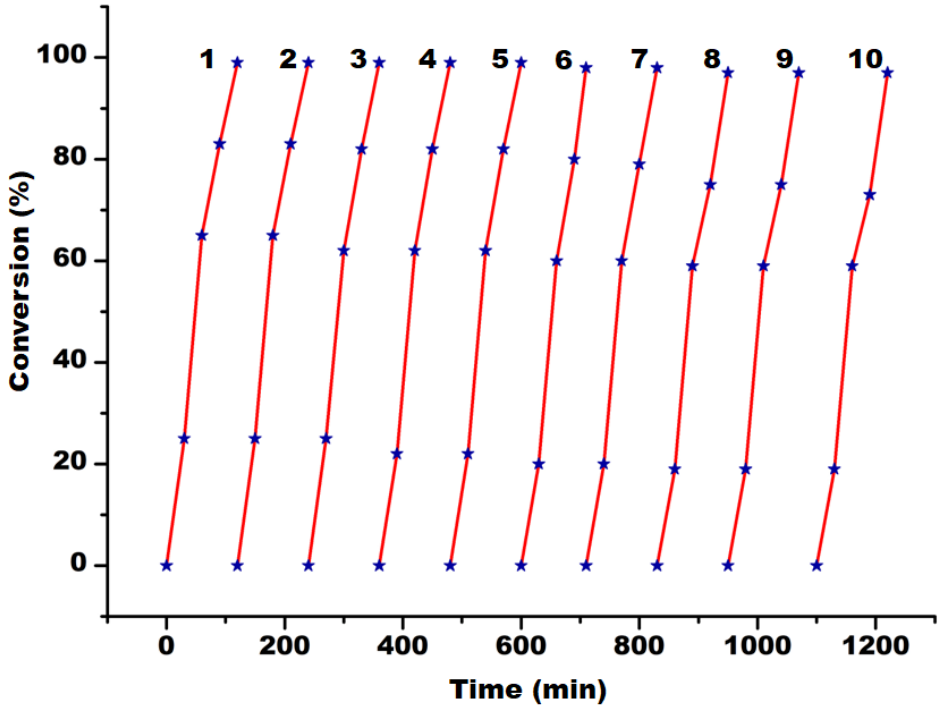

Figure 3.12: The stability study of PdNPs@UCOF-SH catalyst (★ represents different reaction time)

The HRTEM images showed agglomeration of the palladium nanoparticles. It can be clearly observed from the results no change in the characteristic PXRD pattern, FTIR peaks, and elements showed the framework structure remains intact even after 10 catalytic cycles.

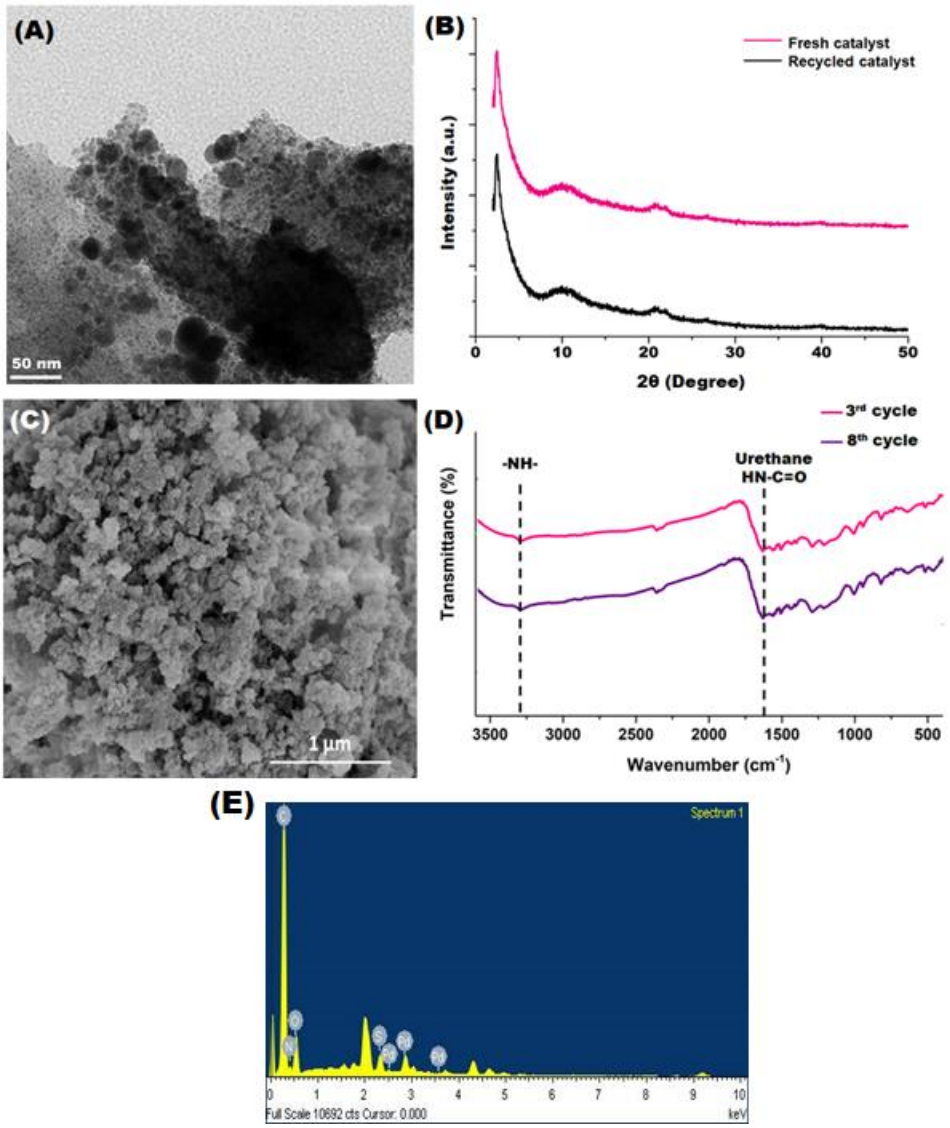

Figure 3.13: Characterization of the recycled catalyst after 8 catalytic runs (A) HRTEM image (B) PXRD pattern (C) FEG-SEM image, (D) FTIR spectra and (E) EDS analysis.

The content of Pd in the catalyst recovered after 10 cycles was found to be 4.06 %. which was very close to that in the fresh catalyst (4.08 %). The hot filtration test was also performed to confirm the heterogeneity of the catalyst. After reacting the model substrates for 1.0 h, PdNPs@UCOF-SH was filtered and the reaction was allowed to proceed under the same reaction conditions. It was observed that no coupling product of biphenyl was obtained even after allowing the reaction for a

longer time **(Figure 3.14).** Moreover, the liquid phase of the reaction mixture was collected after each reaction to test if the palladium was leaching from the solid catalyst during the reaction. ICP-AES analysis confirmed that an extremely low amount of Pd (less than 1.0 ppm) was found in the filtrate. These results indicated that the current reaction was heterogeneous in nature, which may be attributed to the strong bonding between PdNPs and UCOF-SH.

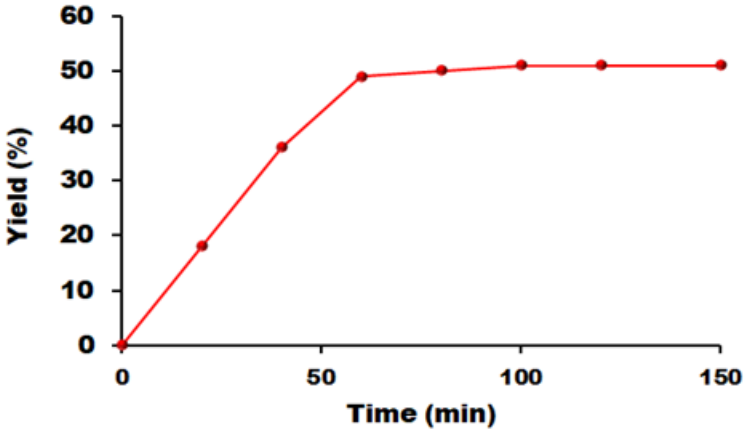

Figure 3.14: Heterogeneity test (Bromobenzene (0.5 mmol), phenylboronic acid (0.75 mmol), 1.0 mmol of Cs_2CO_3, 0.75 mol % of PdNPs@UCOF-SH, and solvent EtOH: H_2O 5 ml).

3.4 Plausible Mechanism

A plausible mechanism was proposed to explain the catalytic phenomenon taking bromobenzene and phenylboronic acid as model reactants as shown in **Figure 3.15**. As shown in the **Figure 3.15**, the reaction occurs at the active site Pd nanoparticle. Initially, in the oxidative addition step, bromobenzene (Ph-Br) diffuses through the porous structure of covalent organic framework support and then reaches the active sites i.e, palladium nanoparticles. Then, the palladium leaching phenomenon occurs from the oxidative reaction between the inner PdNPs@UCOF-SH catalyst and the penetrating Ph-Br, transforming Pd (0) into Pd (II) in organic phase and leading to the formation of surface intermediate Ph-Pd-Br[31]. This intermediate (Ph-Pd-Br) can desorb and then transfer across the porous COF support, joining the reaction system. In water phase, a boronate complex is formed by the ionization of phenylboronic acid in a higher basic water phase (formed by cesium carbonate. Futher, the transmetallation of Ph-Pd-Br and phenylboronic acid would happen unavoidably at water and organic interphase, leading to the formation of biaryl palladium type Ph-Pd (II)-Ph. Finally, the biaryl product Ph-Ph can be formed via the reductive elimination of Pd from the Ph-Pd (II)-Ph intermediate. Simultaneously, the Pd (II) state will be reduced to a

Pd (0) state.

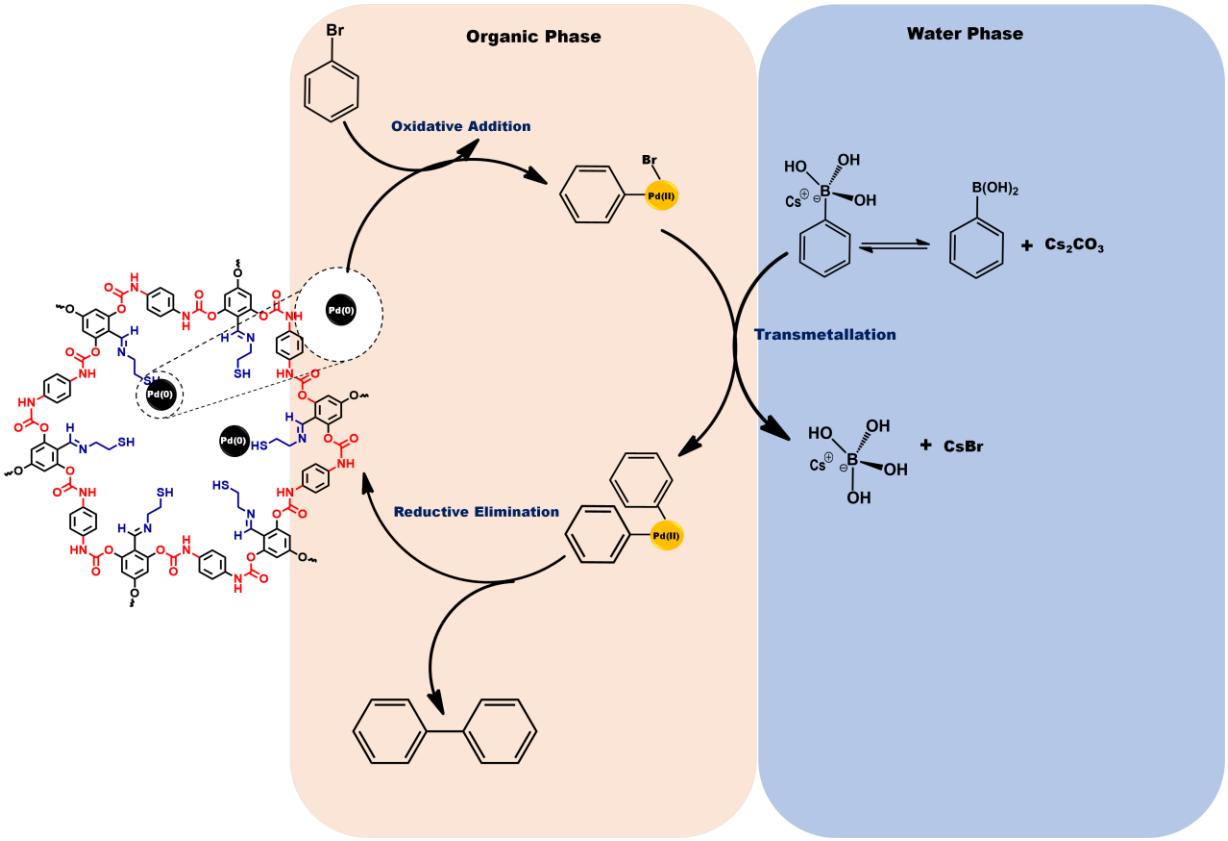

Figure 3.15: Plausible Mechanism of PdNPs@UCOF-SH catalyzed Suzuki Miyuara Cross-Coupling reaction.

3.5 Conclusion

To summarize, this work reports the synthesis and functionalization of a novel urethane-linked covalent organic framework for the first time. The pendant formyl group of UCOF was rationally functionalized using cysteamine to obtain thiol-decorated COF which can assist in the size-controlled synthesis of stable and highly dispersed ultrafine palladium NPs. With the assistance of equally spaced thiol groups in the ordered framework, Pd NPs of small size (4-6 nm) dispersion was acquired successfully. The UCOF-SH stabilized Pd NPs showed excellent catalytic activity in terms of low catalyst loading, high yield, and milder reaction conditions toward the Suzuki cross-coupling reaction in water: ethanol as solvent. Additionally, the catalyst is extremely stable, easily recyclable, and reusable which makes it a potential catalyst for the future catalytic applications in industries.

3.6 References

[1] C.C.C. Johansson Seechurn, M.O. Kitching, T.J. Colacot, V. Snieckus, Palladium-catalyzed cross-coupling: A historical contextual perspective to the 2010 nobel prize, Angew. Chemie - Int. Ed. 51 (2012) 5062–5085. https://doi.org/10.1002/anie.201107017.

[2] C.F.R.A.C. Lima, A.S.M.C. Rodrigues, V.L.M. Silva, A.M.S. Silva, L.M.N.B.F. Santos, Role of the base and control of selectivity in the suzuki-miyaura cross-coupling reaction, ChemCatChem. 6 (2014) 1291–1302. https://doi.org/10.1002/cctc.201301080.

[3] B.S. Kadu, Suzuki-Miyaura cross coupling reaction: recent advancements in catalysis and organic synthesis, Catal. Sci. Technol. 11 (2021) 1186–1221. https://doi.org/10.1039/d0cy02059a.

[4] G. Liu, F. Han, C. Liu, H. Wu, Y. Zeng, R. Zhu, X. Yu, S. Rao, G. Huang, J. Wang, A Highly Active Catalyst System for Suzuki-Miyaura Coupling of Aryl Chlorides, Organometallics. 38 (2019) 1459–1467. https://doi.org/10.1021/acs.organomet.8b00883.

[5] T. Niwa, Y. Uetake, M. Isoda, T. Takimoto, M. Nakaoka, D. Hashizume, H. Sakurai, T. Hosoya, Lewis acid-mediated Suzuki–Miyaura cross-coupling reaction, Nat. Catal. 4 (2021) 1080–1088. https://doi.org/10.1038/s41929-021-00719-6.

[6] T. Ichikawa, M. Netsu, M. Mizuno, T. Mizusaki, Y. Takagi, Y. Sawama, Y. Monguchi, H. Sajiki, Development of a Unique Heterogeneous Palladium Catalyst for the Suzuki–Miyaura Reaction using (Hetero)aryl Chlorides and Chemoselective Hydrogenation, Adv. Synth. Catal. 359 (2017) 2269–2279. https://doi.org/10.1002/adsc.201700156.

[7] K. Geng, T. He, R. Liu, S. Dalapati, K.T. Tan, Z. Li, S. Tao, Y. Gong, Q. Jiang, D. Jiang, Covalent Organic Frameworks: Design, Synthesis, and Functions, Chem. Rev. 120 (2020) 8814–8933. https://doi.org/10.1021/acs.chemrev.9b00550.

[8] C. Xiong, H. Ning, G. Jia, X. Hong, X. Fei, J. Donglin, Towards covalent organic frameworks with predesignable and aligned open docking sites, Chem. Commun. 50 (2014) 6161–6163. https://doi.org/10.1039/c4cc01825g.

[9] T. Kundu, J. Wang, Y. Cheng, Y. Du, Y. Qian, G. Liu, D. Zhao, Hydrazone-based covalent organic frameworks for Lewis acid catalysis, Dalt. Trans. 47 (2018) 13824–13829. https://doi.org/10.1039/c8dt03005g.

[10] S.Y. Jiang, S.X. Gan, X. Zhang, H. Li, Q.Y. Qi, F.Z. Cui, J. Lu, X. Zhao, Aminal-Linked Covalent Organic Frameworks through Condensation of Secondary Amine with Aldehyde, J. Am. Chem. Soc. 141 (2019) 14981–14986. https://doi.org/10.1021/jacs.9b08017.

[11] Q. Guan, G.B. Wang, L. Le Zhou, W.Y. Li, Y. Bin Dong, Nanoscale covalent organic frameworks as theranostic platforms for oncotherapy: Synthesis, functionalization, and applications, Nanoscale Adv. 2 (2020) 3656–3733. https://doi.org/10.1039/d0na00537a.

[12] M.K. Bhunia, S.K. Das, P. Pachfule, R. Banerjee, A. Bhaumik, Nitrogen-rich porous covalent imine network (CIN) material as an efficient catalytic support for C-C coupling reactions, Dalt. Trans. 41 (2012) 1304–1311. https://doi.org/10.1039/c1dt11350j.

[13] J. Shi, T. Zheng, Y. Zhang, B. Guo, J. Xu, Reprocessable Cross-Linked Polyurethane with Dynamic and Tunable Phenol-Carbamate Network, ACS Sustain. Chem. Eng. 8 (2020) 1207–1218. https://doi.org/10.1021/acssuschemeng.9b06435.

[14] J.O. Akindoyo, M.D.H. Beg, S. Ghazali, M.R. Islam, N. Jeyaratnam, A.R. Yuvaraj, Polyurethane types, synthesis and applications-a review, RSC Adv. 6 (2016) 114453–114482. https://doi.org/10.1039/c6ra14525f.

[15] R.L. Wang, D.P. Li, L.J. Wang, X. Zhang, Z.Y. Zhou, J.L. Mu, Z.M. Su, The preparation of new covalent organic framework embedded with silver nanoparticles and its applications in degradation of organic pollutants from waste water, Dalt. Trans. 48 (2019) 1051–1059. https://doi.org/10.1039/C8DT04458A.

[16] Y. Jiang, C. Liu, A. Huang, EDTA-Functionalized Covalent Organic Framework for the Removal of Heavy-Metal Ions, ACS Appl. Mater. Interfaces. 11 (2019) 32186–32191. https://doi.org/10.1021/acsami.9b11850.

[17] S. Ghosh, R.A. Molla, U. Kayal, A. Bhaumik, S.M. Islam, Ag NPs decorated on a COF in the presence of DBU as an efficient catalytic system for the synthesis of tetramic acids via CO 2 fixation into propargylic amines at atmospheric pressure, Dalt. Trans. 48 (2019) 4657–4666. https://doi.org/10.1039/c9dt00017h.

[18] B. Mendoza-Novelo, J.L. Mata-Mata, A. Vega-González, J. V. Cauich-Rodríguez, Á. Marcos-Fernández, Synthesis and characterization of protected oligourethanes as crosslinkers of collagen-based scaffolds, J. Mater. Chem. B. 2 (2014) 2874–2882. https://doi.org/10.1039/c3tb21832e.

[19] S. Ravi, P. Puthiaraj, K.H. Row, D.W. Park, W.S. Ahn, Aminoethanethiol-Grafted Porous Organic Polymer for Hg2+ Removal in Aqueous Solution, Ind. Eng. Chem. Res. 56 (2017) 10174–10182. https://doi.org/10.1021/acs.iecr.7b02743.

[20] Q. Sun, W. Ma, O. Dan, G. Li, Y. Yang, X. Yan, H. Su, Z. Lin, Z. Cai, Thiol functionalized covalent organic framework for highly selective enrichment and detection of mercury by matrix-

assisted laser desorption/ionization time-of-flight mass spectrometry, Analyst. 146 (2021) 2991–2997. https://doi.org/10.1039/d1an00282a.

21] S. Lu, Y. Hu, S. Wan, R. Mccaffrey, Y. Jin, H. Gu, W. Zhang, Synthesis of Ultrafine and Highly Dispersed Metal Nanoparticles Confined in a Thioether-Containing Covalent Organic Framework and Their Catalytic Applications, 2017. http://pubs.acs.org.

[22] D. Pakulski, V. Montes-García, A. Gorczyński, W. Czepa, T. Chudziak, P. Samorì, A. Ciesielski, Thiol-decorated covalent organic frameworks as multifunctional materials for high-performance supercapacitors and heterogeneous catalysis, J. Mater. Chem. A. 10 (2022) 16685–16696. https://doi.org/10.1039/d2ta03867f.

[23] J. Qiu, H. Wang, Y. Zhao, P. Guan, Z. Li, H. Zhang, H. Gao, S. Zhang, J. Wang, Hierarchically porous covalent organic frameworks assembled in ionic liquids for highly effective catalysis of C-C coupling reactions, Green Chem. 22 (2020) 2605–2612. https://doi.org/10.1039/d0gc00223b.

[24] S. Wu, N. Ding, P. Jiang, L. Wu, Q. Feng, L. Zhao, Y. Wang, Q. Su, H. Zhang, Q. Yang, A two-dimensional amide-linked covalent organic framework anchored Pd catalyst for Suzuki-Miyaura coupling reaction in the aqueous phase at room temperature, Tetrahedron Lett. 61 (2020) 152656. https://doi.org/10.1016/j.tetlet.2020.152656.

[25] A.K. Mishra, D.K. Chattopadhyay, B. Sreedhar, K.V.S.N. Raju, FT-IR and XPS studies of polyurethane-urea-imide coatings, Prog. Org. Coatings. 55 (2006) 231–243. https://doi.org/10.1016/j.porgcoat.2005.11.007.

[26] L. Huang, C. Peng, Q. Cheng, M. He, B. Chen, B. Hu, Thiol-Functionalized Magnetic Porous Organic Polymers for Highly Efficient Removal of Mercury, Ind. Eng. Chem. Res. 56 (2017) 13696–13703. https://doi.org/10.1021/acs.iecr.7b03093.

[27] D.G. Castner, K. Hinds, D.W. Grainger, X-ray photoelectron spectroscopy sulfur 2p study of organic thiol and bisulfide binding interactions with gold surfaces, Langmuir. 12 (1996) 5083–5086. https://doi.org/10.1021/la960465w.

[28] H.C. Ma, J.L. Kan, G.J. Chen, C.X. Chen, Y. Bin Dong, Pd NPs-Loaded Homochiral Covalent Organic Framework for Heterogeneous Asymmetric Catalysis, Chem. Mater. 29 (2017) 6518–6524. https://doi.org/10.1021/acs.chemmater.7b02131.

[29] M. Fan, W.D. Wang, Y. Zhu, X. Sun, F. Zhang, Z. Dong, Palladium clusters confined in triazinyl-functionalized COFs with enhanced catalytic activity, Appl. Catal. B Environ. 257 (2019) 117942. https://doi.org/10.1016/j.apcatb.2019.117942.

[30] S.Y. Ding, J. Gao, Q. Wang, Y. Zhang, W.G. Song, C.Y. Su, W. Wang, Construction of covalent organic framework for catalysis: Pd/COF-LZU1 in Suzuki-Miyaura coupling reaction, J. Am. Chem. Soc. 133 (2011) 19816–19822. https://doi.org/10.1021/ja206846p.

[31] J. Liu, H. Zhan, N. Wang, Y. Song, C. Wang, X. Wang, L. Ma, L. Chen, Palladium Nanoparticles on Covalent Organic Framework Supports as Catalysts for Suzuki-Miyaura Cross-Coupling Reactions, ACS Appl. Nano Mater. 4 (2021) 6239–6249. https://doi.org/10.1021/acsanm.1c01038.

[32] A. Dewan, M. Sarmah, P. Bharali, A.J. Thakur, P.K. Boruah, M.R. Das, U. Bora, Pd Nanoparticles-Loaded Honeycomb-Structured Bio-nanocellulose as a Heterogeneous Catalyst for Heteroaryl Cross-Coupling Reaction, ACS Sustain. Chem. Eng. 9 (2021) 954–966. https://doi.org/10.1021/acssuschemeng.0c08315.

[33] S.S. Qin, Z.K. Wang, L. Hu, X.H. Du, Z. Wu, M. Strømme, Q.F. Zhang, C. Xu, Dual-functional ionic porous organic framework for palladium scavenging and heterogeneous catalysis, Nanoscale. 13 (2021) 3967–3973. https://doi.org/10.1039/d1nr00172h.

[34] J. Yang, Y. Wu, X. Wu, W. Liu, Y. Wang, J. Wang, An N-heterocyclic carbene-functionalised covalent organic framework with atomically dispersed palladium for coupling reactions under mild conditions, Green Chem. 21 (2019) 5267–5273. https://doi.org/10.1039/c9gc01993f.

[35] I. Romero-Muñiz, A. Mavrandonakis, P. Albacete, A. Vega, V. Briois, F. Zamora, A.E. Platero-Prats, Unveiling the Local Structure of Palladium Loaded into Imine-Linked Layered Covalent Organic Frameworks for Cross-Coupling Catalysis, Angew. Chemie - Int. Ed. 59 (2020) 13013–13020. https://doi.org/10.1002/anie.202004197.

[36] W. Chen, P. Cai, P. Elumalai, P. Zhang, L. Feng, M. Al-Rawashdeh, S.T. Madrahimov, H.C. Zhou, Site-Isolated Azobenzene-Containing Metal-Organic Framework for Cyclopalladated Catalyzed Suzuki-Miyuara Coupling in Flow, ACS Appl. Mater. Interfaces. 13 (2021) 51849–51854. https://doi.org/10.1021/acsami.1c03607.

[37] M. Ravbar, A. Koler, M. Paljevac, P. Krajnc, M. Kolar, J. Iskra, Reusable Pd-PolyHIPE for Suzuki-Miyaura Coupling, ACS Omega. 7 (2022) 12610–12616. https://doi.org/10.1021/acsomega.1c06318.[38] H. Vardhan, A. Nafady, A.M. Al-Enizi, S. Ma, Pore surface engineering of covalent organic frameworks: Structural diversity and applications, Nanoscale. 11 (2019) 21679–21708. https://doi.org/10.1039/c9nr07525a.

Spectral Data

1,1'-Biphenyl

^{1}H NMR (500 MHz, $CDCl_3$): δ7.58(t, *J*= 7.8 Hz, 4H), 7.41-7.45 (m, 4H), 7.34 (t, *J*=7.5Hz, 2H) ppm

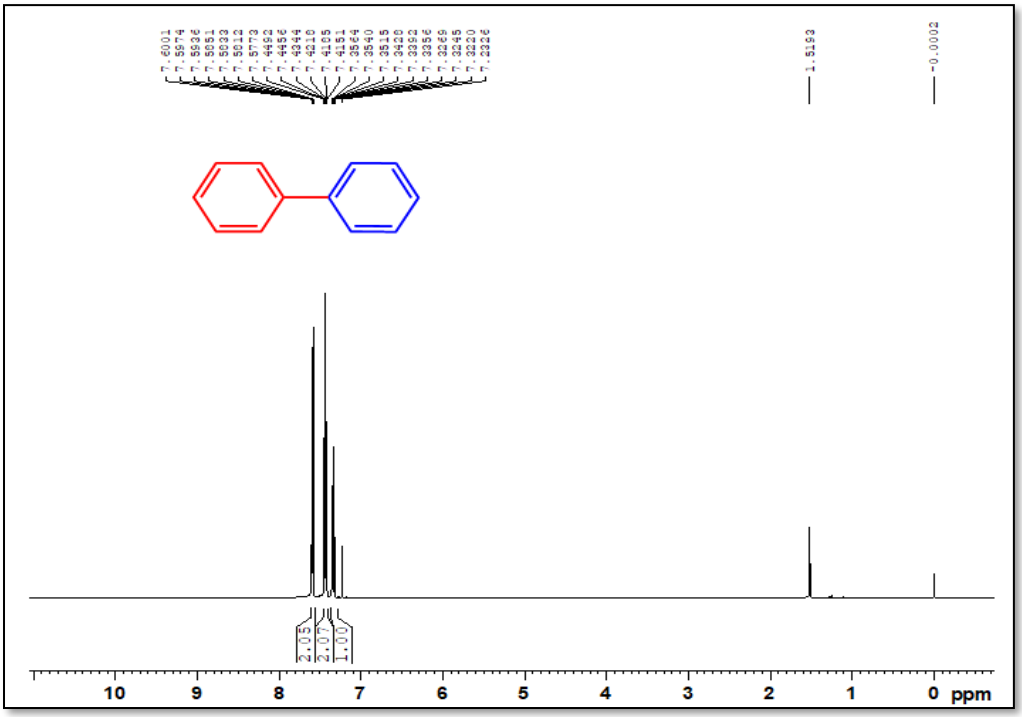

Figure S1:1H NMR of 1,1'-Biphenyl

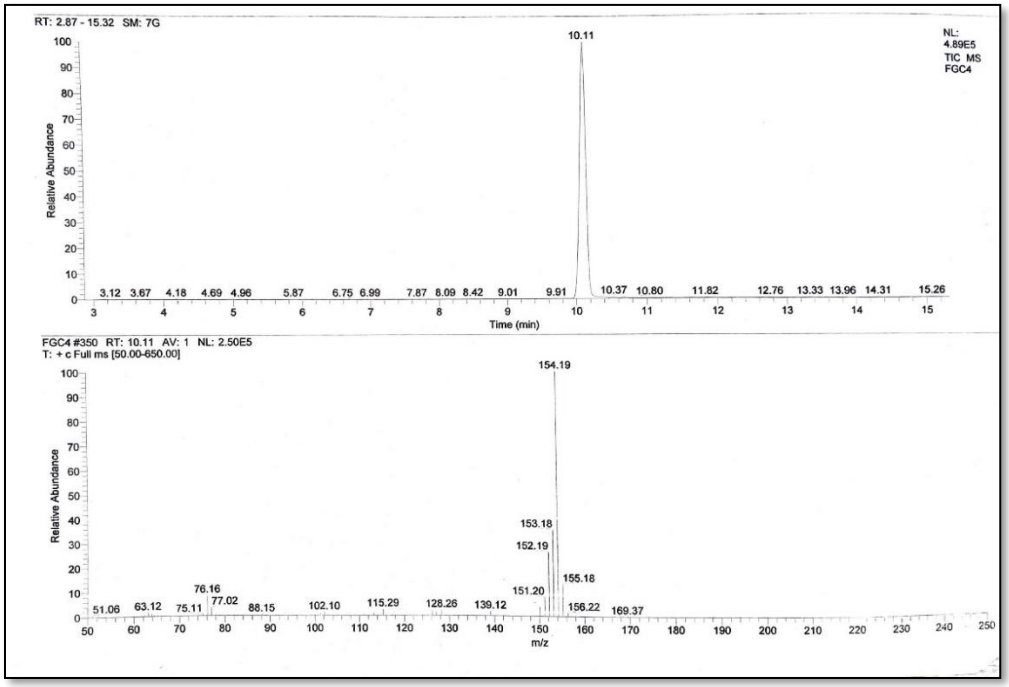

Figure S2: GC-MS spectrum of 1,1'-Biphenyl

4-Methoxy-1,1'-biphenyl

^{1}H NMR (400 MHz, $CDCl_3$): δ 7.57-7.59(m, 4H), 7.48 (t, *J* = 7.5 Hz, 2H), 7.17 (t, *J* = 6.2 Hz, 1H), 6.99 (d, *J* = 8.8 Hz, 2H), 3.88 (s, 3H) ppm.

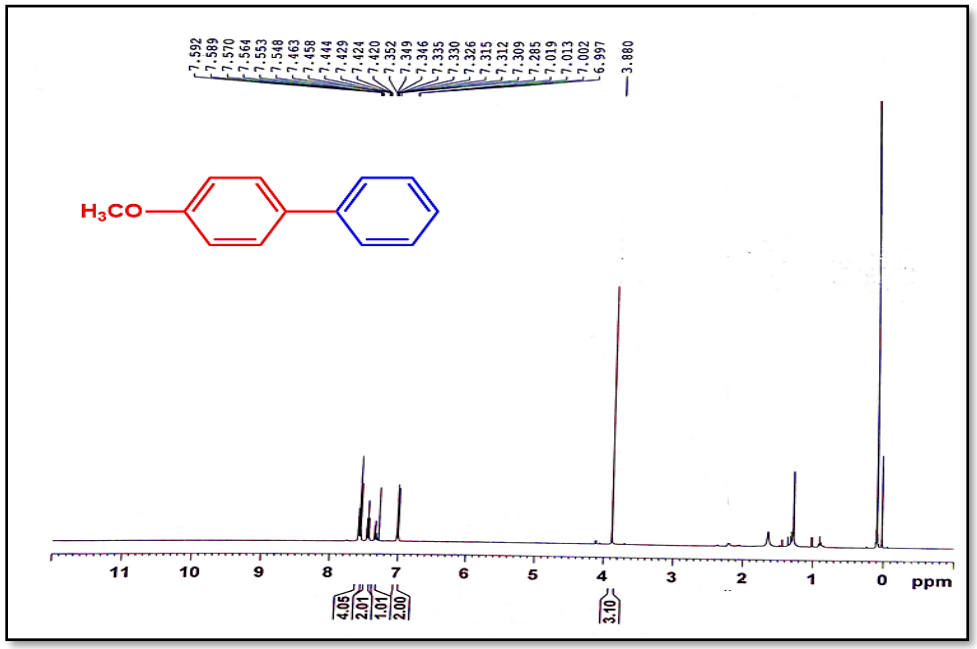

Figure S3: ^{1}H NMR of 4-Methoxy-1,1'-biphenyl

4,4'-Dimethoxy-1,1'-biphenyl

^{1}H NMR (500 MHz, $CDCl_3$): δ 7.33 (d, J = 8.9 Hz, 2H), 6.73 (d, J = 8.9 Hz, 2H), 3.71 (s, 3H) ppm

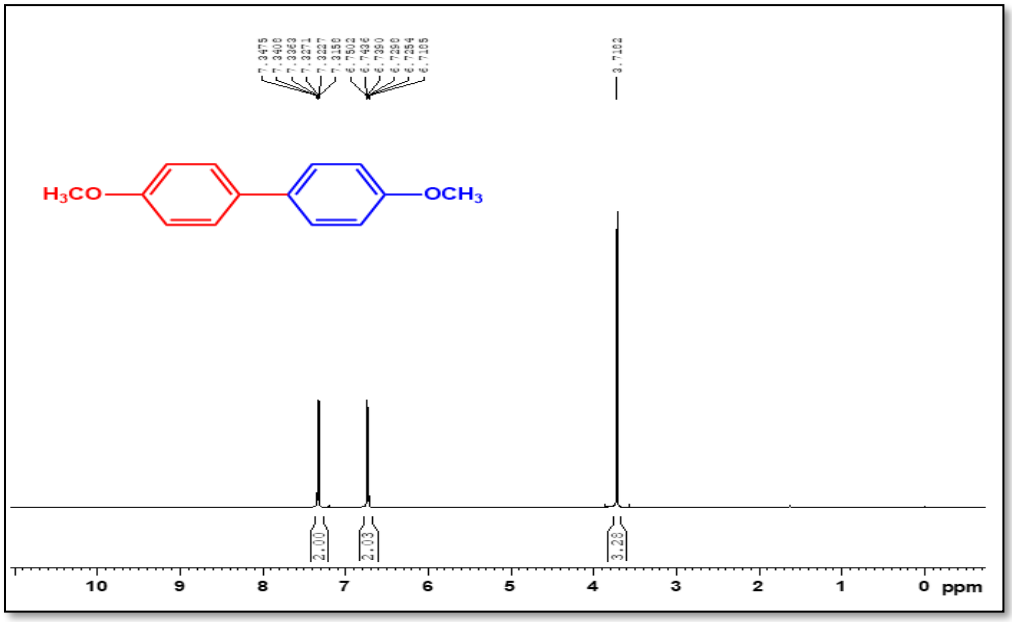

Figure S4: ^{1}H NMR of 4,4'-Dimethoxy-1,1'-biphenyl

4-Acetyl-1,1'-biphenyl

^{1}H NMR (500 MHz, $CDCl_3$): δ 8.02 (d, J = 8.4 Hz, 2H), 7.64 (d, J = 8.4 Hz, 2H), 7.55 (d, J = 8.0 Hz, 2H), 7.46 (d, J = 8.0 Hz, 2H), 7.29 (t, J = 8.0 Hz, 1H), 2.63 (s, 3H) ppm.

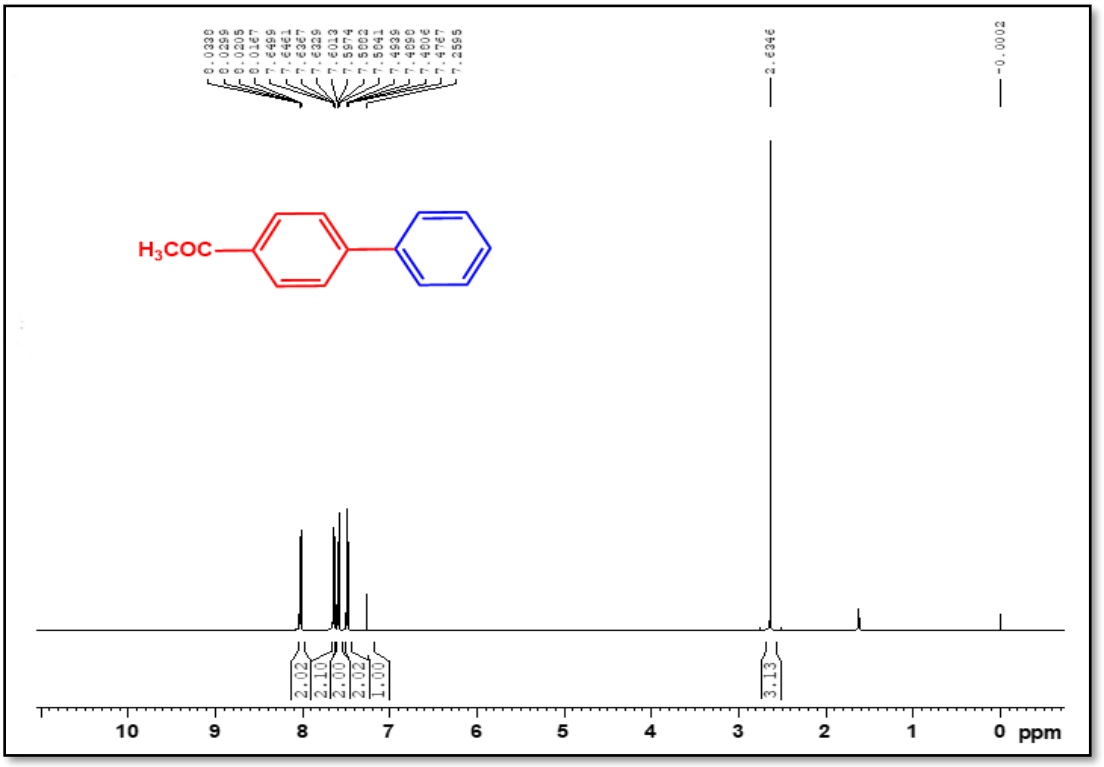

Figure S5: ^{1}H NMR of 4-Acetyl-1,1'-biphenyl

4-Cyano-p-terphenyl

^{1}H NMR (500 MHz, $CDCl_3$): δ 8.12 (t, J= 6.15 Hz, 2H), 7.67 (t, J= 6.4 Hz, 1H), 7.55-7.33 (m,10H) ppm.

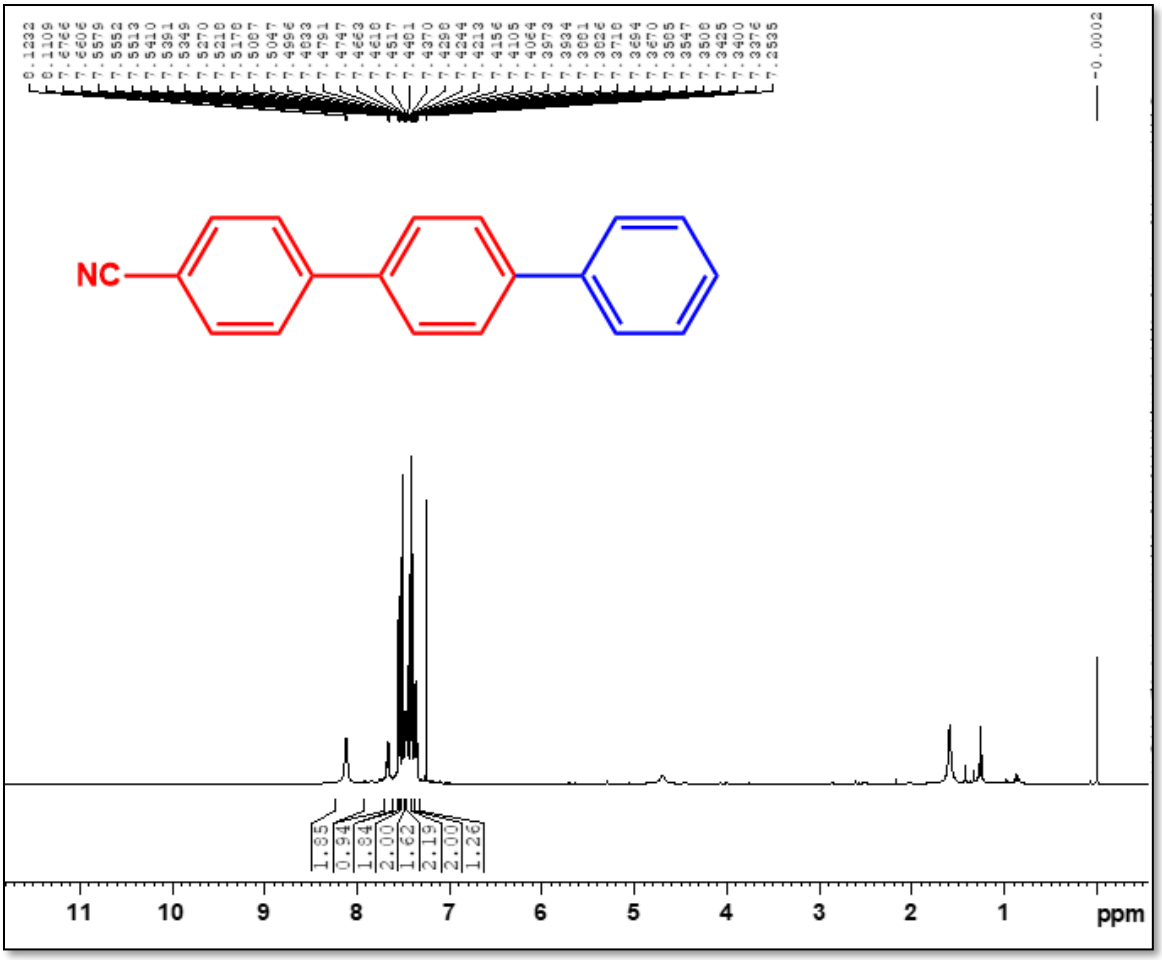

Figure S6: ^{1}H NMR of 4-Cyano-p-terphenyl

3-Flouro-4-nitro-4'-flouro-1,1'-biphenyl

^{1}H NMR (500 MHz, $CDCl_3$): δ 8.23 (d, J=6.85 Hz, 2 H), 7.73 (s, 1H), 7.59 (d, J=7.1 Hz, 1H), 7.59-7.46 (m, 2H), 7.41-7.38(m, 1H) ppm.

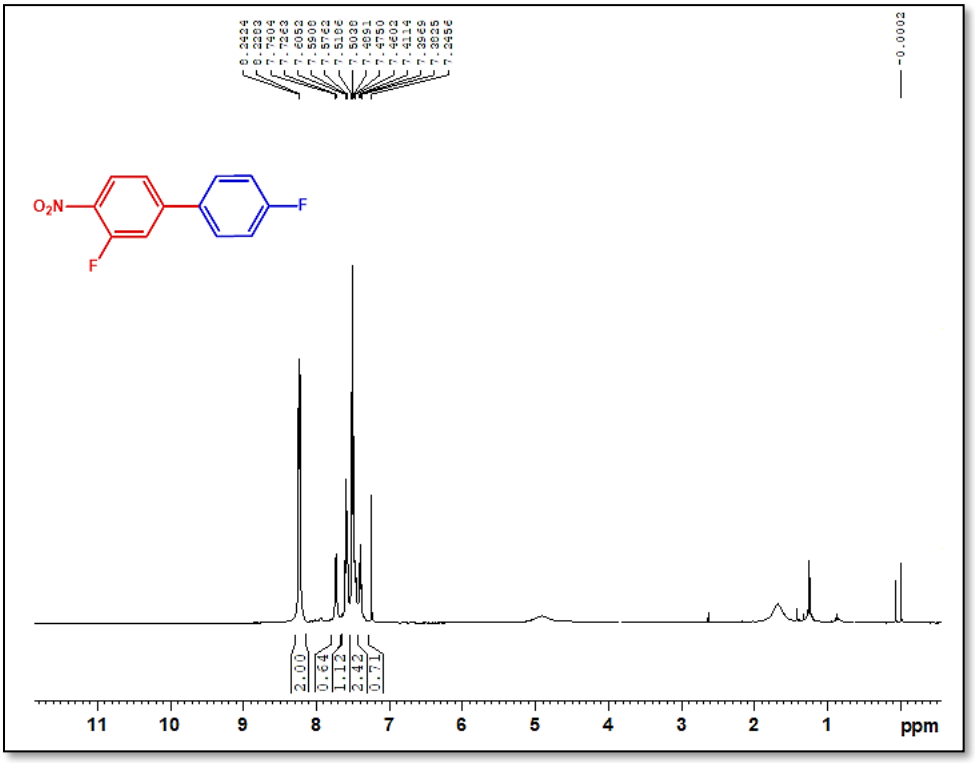

Figure S7: ^{1}H NMR of 3-Flouro-4-nitro-4'-flouro-1,1'-biphenyl

4-Cyano-4'-flouro-1,1'- biphenyl

^{1}H NMR (500 MHz, $CDCl_3$): 7.73-7.64 (m, 4H), 7.49 (d, J = 8.0 Hz, 2H), 7.29 (d, J = 8.0 Hz, 2H) ppm.

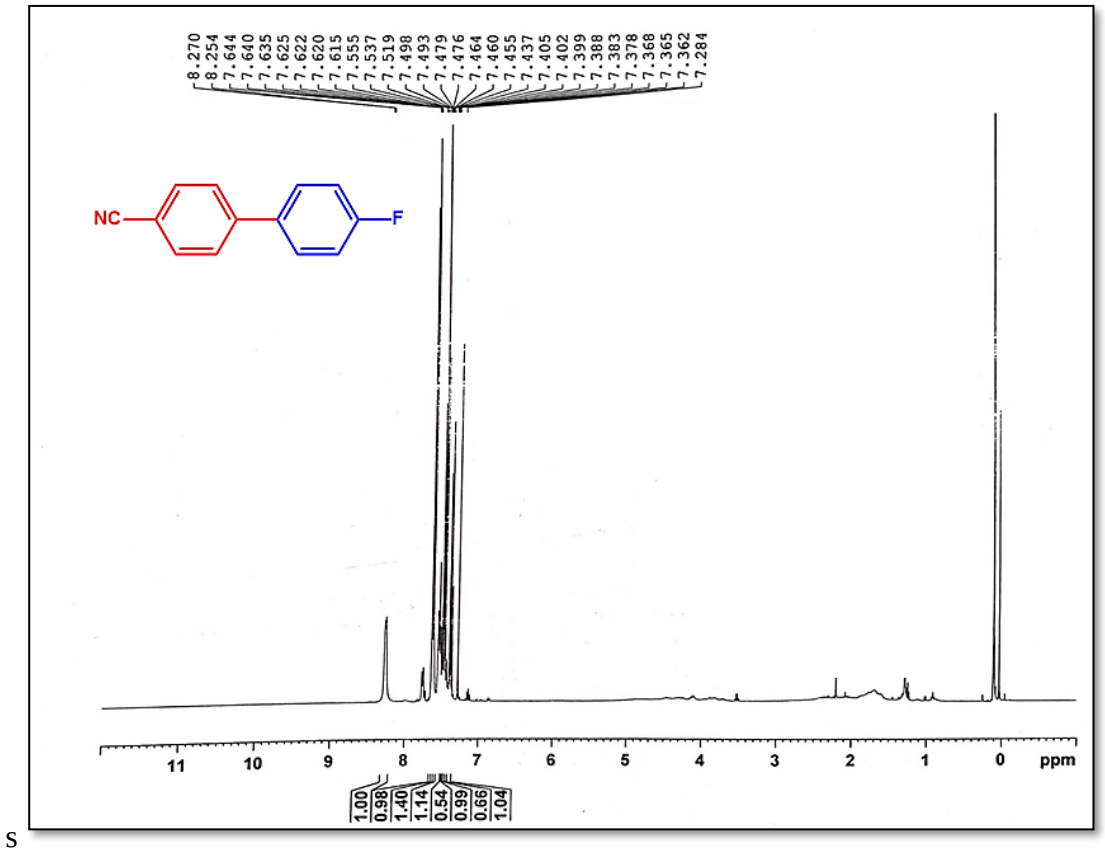

s

Figure S8: ^{1}H NMR of 4-Cyano-4'-flouro-1,1'- biphenyl

4-Methyl-1,1'-biphenyl

^{1}H NMR (400 MHz, $CDCl_3$): δ 2.2 (s, 3H), 7.00 (d, *J* = 8.8 Hz, 2H), 7.33 (t, *J* = 7.6 Hz, 1H), 7.43 (t, *J* =7.8 Hz, 2H),7.51 (m, 4H) ppm.

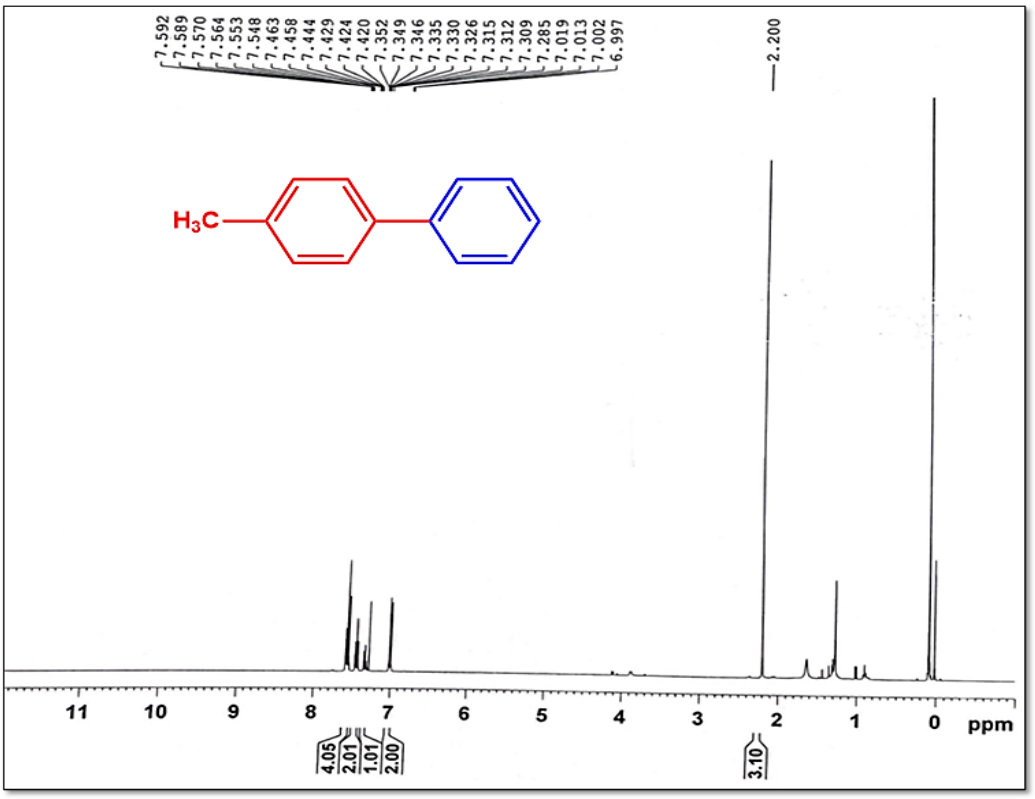

Figure S9: ^{1}H NMR of 4-Methyl-1,1'-biphenyl

4-Flouro-4'-methyl-1,1'- biphenyl

^{1}H NMR (500 MHz, $CDCl_3$): δ 2.63 (s, 3H), 7.48 (d, *J* = 7.5 Hz, 2H), 7.58 (d, *J* = 8.4 Hz, 2H), 7.64 (d, *J* = 8.1 Hz, 2H), 8.02 (d, *J* = 8.5 Hz, 2H) ppm

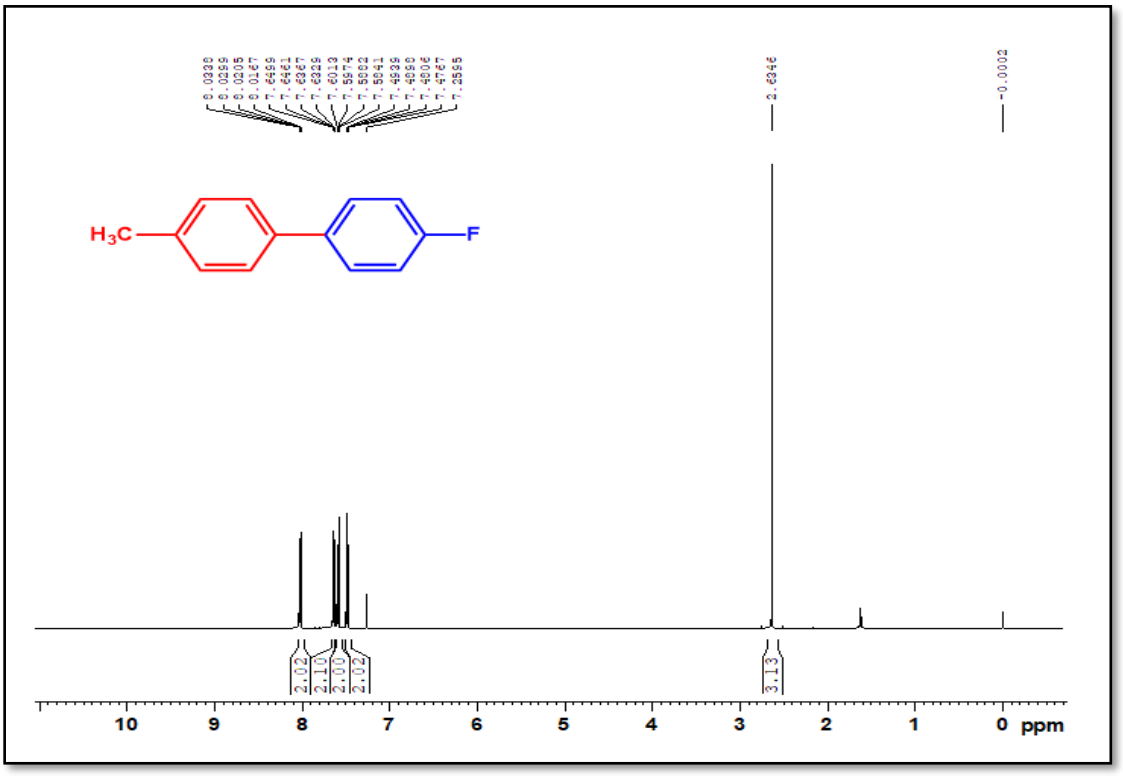

Figure S10: ^{1}H NMR of 4-Flouro-4'-methyl-1,1'- biphenyl